Optimized Energy Management System to Reduce Fuel Consumption in Remote Military Microgrids

Norma Anglani, Giovanna Oriti, and Michele Colombini

***Abstract*—This paper presents an optimized energy management system (OEMS) to control the microgrid of a remote temporary military base (FOB) featuring diesel generators, a battery energy storage system (BESS), and photovoltaic (PV) panels. The information of the expected electric demand is suitably used to improve the sizing and management of the BESS, according to the days of operation. The OEMS includes power electronics to charge the batteries from either the PV source or the diesel generators, and it can function as a current source when it is supplementing the power from one of the generators or as a voltage source when it is the sole source of power for the loads. The new contribution of this paper includes the optimization of a FOB's microgrid, where critical loads must be serviced at all times. The proposed optimization, which uses Special Order Sets for the semicontinuous function handling, also integrates economic evaluations by properly taking into account how the size of BESS affects its charge/discharge cycle; thus, the FOBs' battery lifetime, in addition to its fuel consumption. Results from optimization are employed by the OEMS to coordinate the energy sources, and match the critical and noncritical loads with the available supply. Fuel savings of ≈ 30% (and ≈ 50% adding the PV source) can be achieved with respect to the already improved, but not optimal, solution of a previous work.**

***Index Terms*—Energy management system (EMS), microgrid, mixed integer linear optimization (MILP), rain flow counting method, renewables integration, Special Ordered Set (SOS).**

I. Introduction

RECENT emphasis on energy efficiency has stimulated the use of smart hybrid power supply systems in remote military camps such as the U.S. Marine Corps forward operating bases (FOBs) [1], [2], also in view of new electrifying paradigms [3]. Reducing fuel consumption results both in reduced operational cost for the FOB, and it can also save soldiers' lives because fuel transportation is dangerous, especially outside U.S. borders. Recently developed FOBs' power systems include a battery energy storage system (BESS) and renewable energy sources such as photovoltaic (PV) panels in addition to traditional diesel generators [4]. In [2], a power electronics based energy management system (EMS) was used to significantly reduce fuel consumption in a power system featuring two diesel generators and a BESS; however, the study did not consider the BESS state of charge (SOC), lifetime, cost, or the addition of PV sources recently introduced in FOBs. In this paper, an optimized EMS (OEMS) is presented where a simple but robust algorithm manages the diesel generators, the BESS, and PV source as shown in Fig. 1.

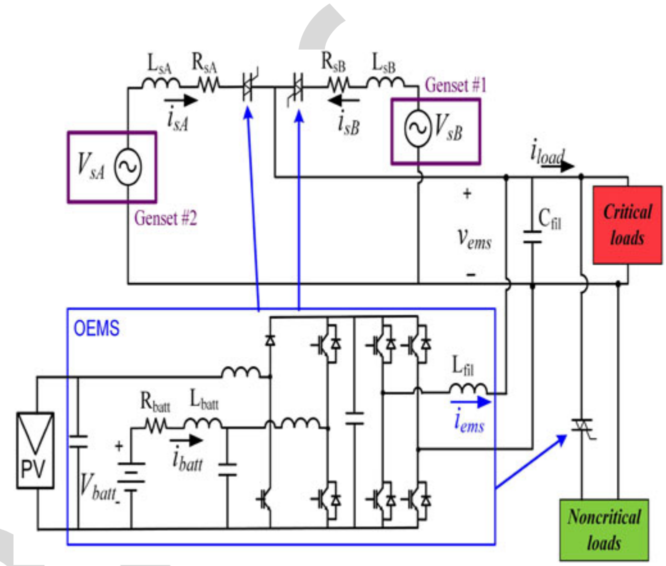

Fig. 1. Optimized energy management system architecture.

Critical loads in the schematic are those electrical devices that must be powered at all times to ensure the success of the military operation. The optimization strategy includes lifetime and economic considerations for the BESS; thus, managing the cost of the microgrid while reducing fuel consumption. Applications of online and offline optimization techniques in the management of energy supply and demand are widely available as in [5], [6], and [7] and more recently in [8] and [9]. They are applied not only to microgrids, as in [10], but also to assess the impact on bigger energy system, as in [11]. Although some of these papers deal with critical load service and fuel consumption, none of them addresses remote military microgrids and their key issues. In the knowledge of the authors, few examples have been able to achieve such amount of savings, by making the optimization problem as simple as it is shown. Supported by the work of Camponogara *et al.* [12], with respect to the use of the Special

Manuscript received October 28, 2016; revised March 14, 2017 and May 8, 2017; accepted July 7, 2017. Paper 2016-SECSC-1156.R2, presented at the 2016 IEEE Energy Conversion Congress and Exposition, Milwaukee, WI, USA, Sep. 18–22, and approved for publication in the IEEE Transactions on Industry Applications by the Sustainable Energy Conversion Systems Committee of the IEEE Industry Applications Society. *(Corresponding author: Norma Anglani.)*

N. Anglani is with the University of Pavia, Pavia 27100, Italy (e-mail: nanglani@unipv.it).

G. Oriti is with the Naval Postgraduate School, Monterey, CA 93943 USA (e-mail: goriti@nps.edu).

M. Colombini is with the Generac Mobile Product srl, Villanova d'Ardenghi 27030, Italy (e-mail: mich.colombini@gmail.com).

Color versions of one or more of the figures in this paper are available online at http://ieeexplore.ieee.org.

Digital Object Identifier 10.1109/TIA.2017.2734045

Ordered Sets (SOSs) and by the work of Tankari *et al.* (2013) in the use of the rainflow counting method [13], we tailored the algorithms and match them together to find a solution to the problem of minimizing the fuel consumptions of the FOBs and optimize the BESS size, according to the operating days. No previous work solved the specific problems of a FOB, except [14], which proposes the use of HOMER, but with different purposes. In this paper, a well-known mixed integer linear programming (MILP) formulation is proposed for the OEMS. Although MILP is less sophisticated than other algorithms available in the literature, analysis shows that its robustness is a fundamental asset to speed up controlling strategies and obtain satisfactory results.

The new contribution of this paper includes the overall optimization procedure which uses SOSs for the semicontinuous function handling, and integrates economic evaluations by properly taking into account how the size of BESS affects its charge/discharge cycle; thus, the battery lifetime. Another new contribution is the hardware implementation of the optimized control system; in a laboratory prototype the OEMS coordinates the energy sources and BESS to service critical and noncritical loads using the results from the proposed optimization. It should be noted that the application of microgrid technology to FOBs is rarely found in the literature, therefore this paper is also new in the application that it presents. One important variable that must be considered in a FOB is that critical loads must be serviced at all times, even if this results in shedding of noncritical loads when a fault occurs. With the proposed algorithm, we operate to avoid the shedding. Two optimized scenarios, with and without a PV source, demonstrate fuel savings of $\approx 30\% - 50\%$, respectively, compared to previous work [2]. The scenarios approach supports a sensitivity analysis on the amount of savings, when the PV production may fail. Experimental measurements demonstrate the OEMS functionality.

In Section II, the power electronics based OEMS will be illustrated. In Section III, the formulation of the optimization problem, the methodology based on SOS-constraints, and the rainflow counting method are presented to solve the minimization of the fuel consumption and for the optimal sizing of the BESS. The case study and the sizing are described and solved in Section IV, according to the operating days, conclusions are drawn in Section V.

II. Power Electronics Based EMS

The EMS depicted in Fig. 1 includes three inverter legs and a field programmable gate array (FPGA) based control system. Two of the legs are used for a bidirectional H-bridge converter which converts power from the dc bus to the ac loads and vice-versa. The other two legs are used for the battery pack and PV panels, respectively. Since the PV source power flows unidirectionally, only one switch and one diode of the fourth inverter leg are used for the boost converter that conditions the PV power. The EMS includes a primary controller [15] for the power electronics and a secondary controller to manage the loads and distributed resources, including storage and PV. Solid state switches are used to connect and disconnect the two generator sets (gensets) and the noncritical loads, which can be shed if there is a power failure or to control peak power consumption. While Oriti *et al.* [15] focus on the EMS primary control system, this paper focuses on the secondary controller which gives the OEMS the ability to optimally manage loads and the BESS SOC.

III. Problem Formulation: MILP, SOSs, and the Rainflow Counting Method

In the following, we explain how we combine two techniques to provide an optimized secondary control law, able to answer the questions.

1) Which is the best configuration to save fuel and size batteries in a FOB, according to the number of operating days?
2) Which is the range of savings, if PV panels are used?
3) How can we realize it?

At first, we propose a formulation which improves the original setup reported in [2], second, we evolve toward a hybrid microgrid configuration, by adding the new PV plant and finally we optimize the size of the battery according to the economics and the life time of the microgrid (i.e., the operative days of the base). The results of such constrained optimization problem become instrumental for the OEMS described in the previous section. We look at a typical day, divided into *j*th time steps, then we base our model on two vectors of semicontinuous, nonnegative decision variables: $x_{1,j}$ and $x_{2,j}$ the average load factors of genset #1 (P_{1r}=5 kW, rated power) and genset #2 (P_{2r}=15 kW), as defined in (1.5) of Table I.

One interesting feature in our formulation is represented by the choice to also use, as decision variable, the SOC value at the beginning of the day and impose to have the same value at the end of the day. Such choice allows us to take into account the temporal continuity, while representing a typical day. This is a neglected aspect in many papers dealing with optimization on daily profiles, although it is an important one.

Fig. 2 reports the linearized relationships between gensets' consumption (gal/h, 1gal = 3.79 l)) and $x_{i,j}$ (and also power). Data are elaborated from an extensive research on technical datasheets from several manufacturers' websites like Caterpillar [16], Cummins [17], Kohler [18], providing gensets of suitable size for the proposed case study. Although it may seem simple to draw such relationship, a considerable effort is represented by how such data are sought and interpreted from technical datasheets.

We formulate an optimization problem to minimize the fuel consumption of the facility of Fig. 1, that is

$$f(x_{1,j}, x_{2,j}) = \sum_{\substack{1\le i\le 2\\ 1\le j\le J^*}} C_{i,j} = \begin{cases} m_i \cdot x_{i,j} + q_i & \text{when } x_i^m \le x_{i,j} \le x_i^M \\ 0 & \text{when } x_{i,j} = 0 \end{cases} \quad (1)$$

over a J^* horizon, discretized in j time steps. m_i and q_i are the coefficients of the two linear equations in $x_{i,j}$ of the upper Fig. 2. Additional equations describing the working conditions of the diesel gensets and BESS, also with respect to photovoltaic availability, are reported in Table I with a succinct description.

TABLE I
LIST OF VARIABLES, PARAMETERS, AND EQUATIONS DESCRIBING THE PROBLEM CONDITIONS (AT TIME j)

Variable /parameter	Description of var./param. and/or Eq.	Equations	#
$x_{1,j}$ - $x_{2,j}$	dominion of decision variables (i.e., load factors)	$x_1^m \leq x_{1,j} \leq 1$ or $x_{1,j} = 0$ $x_2^m \leq x_{2,j} \leq 1$ or $x_{2,j} = 0$	(1.2)
	no syncro condition	$x_{i,j} > 0 \rightarrow x_{k,j} = 0 \quad \forall k \neq i$	(1.3)
$x_{3,j}$	battery load factor dominion	$-1 \leq x_{3,j} \leq 1$	(1.4)
$P_{i,j}$	power from gen. and from/to BESS at time j (P_{1r}, P_{2r}, P_{BATmax})	$x_{i,j} = \dfrac{P_{i,j}}{P_{ir}}$	(1.5)
T_{bat}, E_{bat}	time of discharge at rated P_{BATmax} and capacity of BESS	$E_{\text{bat}}=P_{\text{BATmax}} \cdot T_{\text{bat}}$	(1.6)
L_j, $P_{PV,j}$	Load and available PV power	$x_{1,j} \cdot P_{1r} + x_{2,j} \cdot P_{2r}$ $-x_{3,j} \cdot P_{\text{BATmax}} + (P_{PV,j})=L_j$	(1.7)
SOC_j in %	state of charge	$SOC_j = SOC_{j-1} + x_{3,j} \cdot \dfrac{j}{T_{\text{bat}}}$	(1.8)
	decision var.	$SOC_0 = SOC_{J^*}$	(1.9)
	dominion	$SOC^m \leq SOC_j \leq SOC^M$	(1.10)

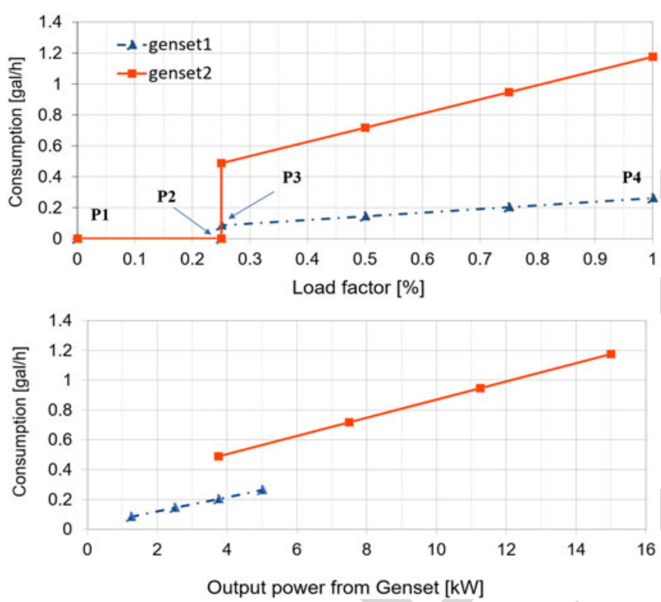

Fig. 2. Fuel consumptions (gal/h) versus load factor (%, or output power in kW) for genset #1 $P_{1,r} = 5$ kW and genset #2 $P_{2,r}$ =15kW. At the top, the coefficients of the linear equations are $m_1 = 0.2366$ - $q_1 = 0.0253$; $m_2 = 0.9153$. $q_2 = 0.2597$, respectively. Elaboration from [16]–[18].

The constraint, involving $\mathbf{x_3}$ a dependant variable, means that the battery can be charged and discharged (assuming both positive and negative values), having as its hourly limit $\pm P_{\text{BATmax}}$. This condition is set to preserve its lifetime, besides charging and discharging efficiencies are set equal to 1.

In balancing the supply and the demand side, also the contribution of the PV source ($P_{PV,j}$) can be taken into account in a deterministic way, if it exists.

If one of the two diesel generators can be used as a backup power to improve the reliability, no synchronization between the two gensets is required, at this stage [19].

Unfortunately (1) and some constraints in Table I are not straightforwardly applicable to linear programming solvers like CPLEX. The objective function (1) is a sum of the consumption associated with the running of the two gensets

$$\begin{cases} f(x_{1,j}) = 0.2366x_{1,j} + 0.0253 \\ f(x_{2,j}) = 0.9153x_{2,j} + 0.2597 \end{cases} \tag{2}$$

in each time frame jth a new $x_{i,j}$ is assessed. $x_{i,j}$ can either be a value between 0.25 and 1 or be 0, so for each function $f(x_i)$, four major points can be identified by their coordinates: $P_i^1(0,0)$, $P_i^2(0.25^-,0)$, $P_i^3(0.25^+, m_i 0.25 + q_i)$, $P_i^4(1, m_i + q_i)$ (see Fig. 2 where the points are highlighted only for genset #1). Besides, the no synchronization requirement implies that at the time j, $\forall i$

$$x_{i,j} > 0 \Leftrightarrow x_{l,j} = 0 \text{ for } l \neq i. \tag{3}$$

To deal with such features on decision variables, the Special Ordered Sets (SOSs), a tool in the Branch and Bound method to branch groups of variables, are introduced [20]. SOSs of type 2 are functional to deal with piecewise linear continuous functions (like the objective function) and type 1 to deal with the no syncronization requirement as in [21] and [22]. The formulation of a MILP problem is thus given, from the objective function of (1) through the definition of all the conditions expressed in Table I.

A. SOSs Type 2 and Type 1 Resolution

SOS2 is an ordered set of nonnegative variables, where *no more than two adjacent elements can be nonzero* in a feasible solution. Consider $f(y)$, the piecewise linear function in y defined in closed intervals $[\hat{y}_k, \hat{y}_{k+1}]$, where $[\hat{y}_k, f(\hat{y}_k)]$ represent the coordinates of $P_1, ..., P_K$ and $k = 1, ..., K$ (Fig. 3)

y in $[\hat{y}_k, \hat{y}_{k+1}]$ can be written as

$$y = \lambda_k \hat{y}_k + \lambda_{k+1} \hat{y}_{k+1} \tag{4}$$

where

$$\lambda_k + \lambda_{k+1} = 1 \quad \text{and} \quad \lambda_k, \lambda_{k+1} \geq 0. \tag{5}$$

As well, $f(y)$, linear in the interval, can be written as

$$f(y) = \lambda_k f(\hat{y}_k) + \lambda_{k+1} f(\hat{y}_{k+1}) \tag{6}$$

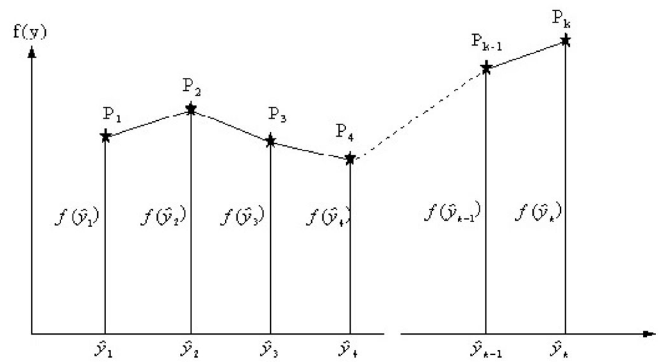

Fig. 3. Generic piecewise linear function $f(y)$ [20].

$f(y)$ can be represented by using a set of *weight* variables λ_k, $k = 1, ..., K$ as

$$f(y) = \lambda_1 f(\hat{y}_1) + \lambda_2 f(\hat{y}_2) + ... + \lambda_K f(\hat{y}_K) \quad (7)$$

where

$$\hat{y}_1\lambda_1 + \hat{y}_2\lambda_2 + ... + \hat{y}_K\lambda_K - y = 0 \qquad y \geq 0 \quad (8)$$

$$\lambda_1 + \lambda_2 + ... + \lambda_K = 1 \qquad \lambda_k \geq 0 \quad k = 1, ..., K. \quad (9)$$

Besides, we must consider the additional condition that no more than two adjacent variable can be nonzero at any time (according to [21] and [22]). These weight variables are the Special Ordered Set type 2.

In an electrical grid, stability is a very important issue as well as redundancy of the supply system: to provide those two requirements for a limited supply system like a FOB can be, where only a few diesel generators exist, we have been assuming that only one generator is running at a time. Taking into account such condition requires the use of SOS1. SOS1 are a set of adjacent subsequent variables where at most one element can be non zero in a feasible solution. Therefore, (9) under the condition of SOS1, that only one element can be nonzero, implies that only one element will be equal to one.

B. Rainflow Counting Method

The addition of batteries and PV sources to a traditional FOB power system leads to fuel savings and CO_2 emission reduction. As the battery size increases the fuel consumption may decrease, but the overall cost of the microgrid will go up. Therefore, battery cost and lifetime must be included in the optimization. In the economic evaluation of a given layout, the real lifetime of a battery is a sensitive parameter depending on the aging, according to the charge/discharge cycles and the DoD (Depth of Discharge). Thus, another step deals with the best sizing of the BESS, according to the typical daily working cycles. The chosen approach was an adaptation of the Miner's Rule [23], introduced by Facinelli in [24]: in brief, he observed that the higher the DoD the lower the lifetime of a battery (see Fig. 4).

Such rule is valid as long as the cycles do not overlap, which is typical of a simple PV+BESS configuration. When the cycles are more irregular, then the rule can not be applied as it is. For instance, this irregularity has been first found in modeling

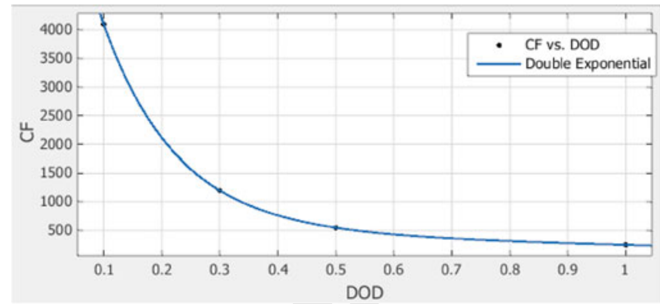

Fig. 4. Fitting curve C_F representing the cycles to failure (lifetime) of batteries versus the fractional DoD, according to data in Table II.

TABLE II
NUMBER OF CYCLES VERSUS DOD FOR LEAD–ACID BATTERIES [29]

Depth of Discharge	# cycle (approx.)
100%	250
50%	550
30%	1200
10%	4100

Investment Costs: $1kW$ = 3250$; 1.5 kW = 4125$; $3kW$ = 6750$; 5 kW=10250$

wind/diesel kind of systems [25]. If overlapping and irregular cycles occur, the Rainflow Count, deriving from the original work of Collins [26], later resumed by [27], [28], and [13], can be used.

The modeling of the wearing out of batteries due to the cycles of charge/discharge is based on considering the lifetime (cycles to failure) depending on the DoD. According to the details in Table II, the fitting curve is identified and drawn in Fig. 4.

The life fraction is $1/C_F$, if after a given number of cycles the sum of the number of the cycles (N_i) multiplied by the life fraction is greater than 1, then the battery is considered being dead. In other words, the fractional damage *D*, defined as

$$D = \sum_{i=1}^{m} \frac{N_i}{C_{F,i}} \quad (10)$$

is the inverse of the lifetime. The unit of measure depends on how the time horizon cycles are counted: if the DoD cycles are evaluated on a single day, then the lifetime of the battery is counted in days. The lead–acid battery characteristics of Section IV are from [29] and are reported in Table II, along with some costs, useful in the case study.

The technique is based on the work of Downing *et al.* [30] and uses an algorithm created by Nielsony in MatLab code [31], where individual cycles and the range of cycles of batteries are assessed according to what is detailed in Section IV. Although the method is conceptually reasonable and it consists of the separation of cycles it must be pointed out that there is no experimental validation of it.

IV. Results for the Case Study of a FOB

This section demonstrates that the optimized algorithm embedded in the OEMS' secondary controller reduces the overall

TABLE III
RELEVANT INPUT AND OUTPUT DATA FOR BOTH THE SCENARIOS (ON A TYPICAL DAY $J^* = 24$)

Description	Scenario n.1 (no PV)	Scenario n.2 (with PV)
input		
$x_{1,j}$ - $x_{2,j}$	0 or 0.25 ÷ 1 (semicont.)	0 or 0.25 ÷ 1 (semicont.)
$x_{3,j}$	$-1 \div 1$	$-1 \div 1$
P_{1r}-P_{2r}-P_{BATmax} in kW	$5 - 15 - 3$	$5 - 15 - 3$
T_{bat} in h (@ $P_{\text{BATmax}} = 3kW_P$)	6	6
SOC^m-SOC^M in $kWh(and\%)$	3.6–18 (20%–100%)	3.6–18 (20%–100%)
P_{PV} peak power in kW	0	3
output		
$SOC_0 = SOC_{24}$ in %	40%	100% (see Figs. 9 and 10)
Consump. in gal/day (savings in %)	7.7 (31%)	4.65 (58%) (see Figs. 7 and 8)

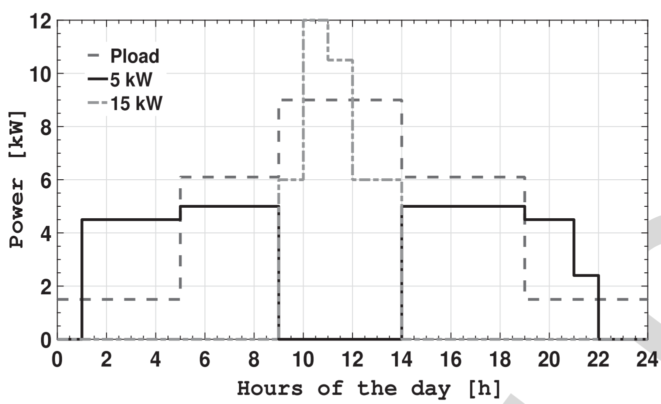

Fig. 5. Scenario n.1: Load and Power from generators (P_{BATmax} equal to 3 kW, $\text{SOC}_0 = \text{SOC}_{24}$, no PV).

cost of the microgrid by including battery lifetime expectation and a load management algorithm, more sophisticated than the one presented in [2]. The experimental results are also illustrated.

A. Optimization and Cost Analysis: The Two Scenarios

In Table III, the most relevant input data are listed for two scenarios: the first without a PV panel, to compare results with the analysis in [2], the second with a 3 kW$_P$ PV panel. At the bottom of Table III, the most important outcomes from the optimization are reported: the optimal initial SOC, the consumption (gal/h), and the savings (%) against the original configuration, where 11.2 gal/day (42.4 l/day) were consumed with the same set of electrical loads [2]. We use two scenarios also to perform a sensitivity analysis and to report a range of savings in case the PV panels work or not.

The results of the two scenarios are reported in details from Figs. 5 to 10. Figs. 5 and 6 show the power curves over a 24 h period for the load, for the two gensets and for the PV source (only in Scenario n.2). In Scenario n.1, both gensets are used but never at the same time; in Scenario n.2, the OEMS chooses to use only genset #1, leaving genset #2 off. This is the result of the optimization algorithm matching the loads to

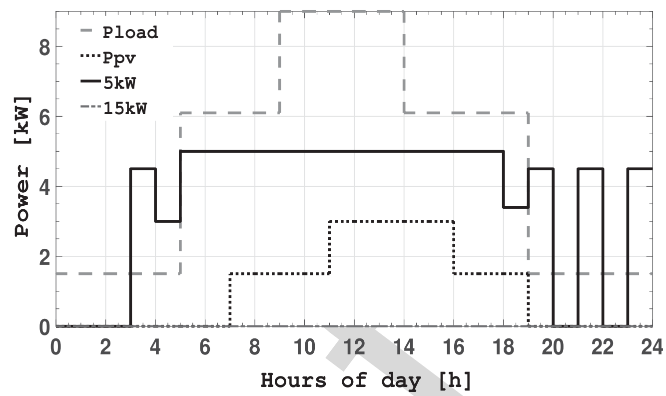

Fig. 6. Scenario n.2: Load and Power from generators (PV and P_{BATmax} both equal to 3kW, $\text{SOC}_0 = \text{SOC}_{24}$).

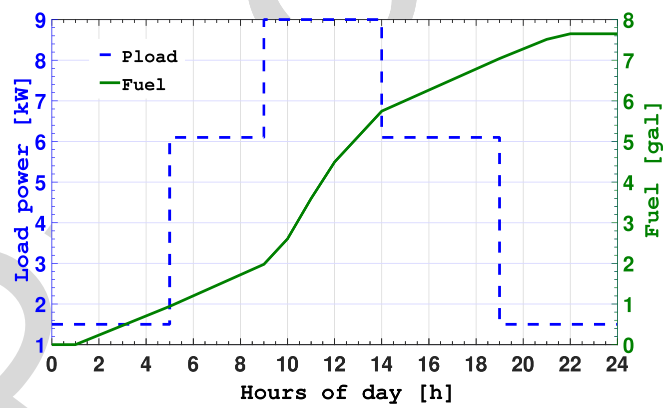

Fig. 7. Scenario n.1: Load and Consumption, power in (kW) on the primary *y-axis*, consumption in (gal) on the secondary *y-axis* (P_{BATmax} equal to 3kW, $\text{SOC}_0 = \text{SOC}_{24}$, no PV).

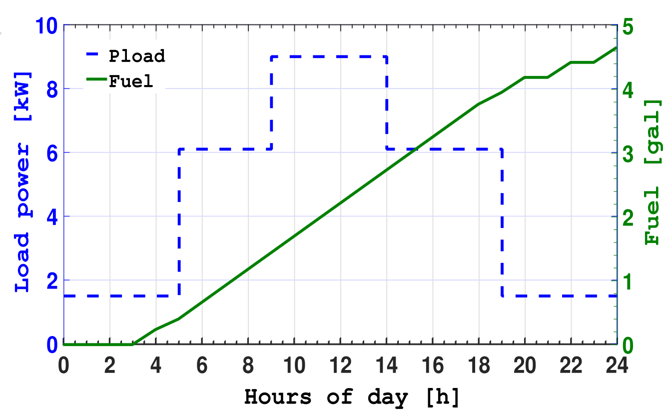

Fig. 8. Scenario n.2: Load and Consumption, power in (kW) on the primary *y-axis*, consumption in (gal) on the secondary *y-axis* (PV and P_{BATmax} both equal to 3kW, $\text{SOC}_0 = \text{SOC}_{24}$).

the sources to minimize fuel consumption, with the addition on security of supply. The fuel consumption over the 24 h period is plotted in Figs. 7 and 8. The total consumed fuel is 7.7 (29.15 l) and 4.65 gallons (17.6 l), which demonstrates in both cases a 31% and 58% reduction, compared to the analysis in [2]. These results demonstrate that the 80% derating practice, typically used when sizing diesel generators in FOBs, is not necessary,

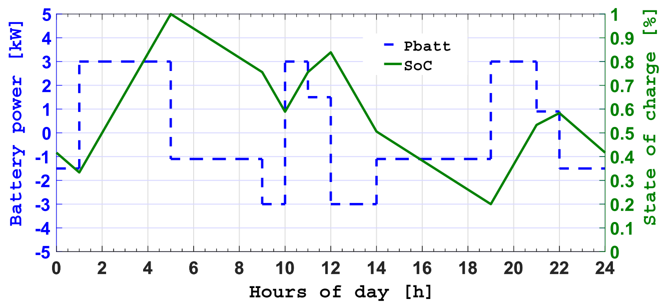

Fig. 9. Scenario n.1: Power from/to Batteries in (kW) (on primary *y-axis*); SOC [%] (on secondary *y-axis*) ($P_{\mathrm{BATmax}} = 3$kW, SOC$_0$=SOC$_{24}$, no PV). On the *x-axis* the hours of the typical day.

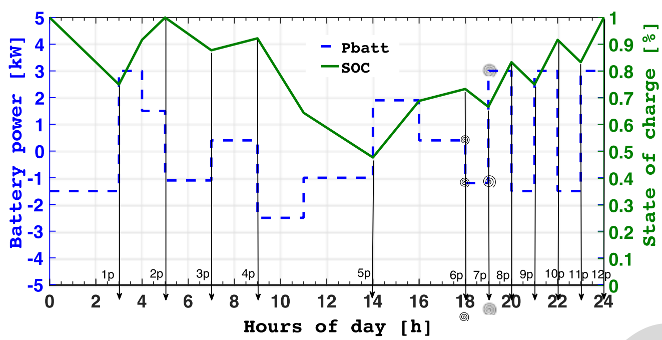

Fig. 10. Scenario n.2: Power from/to Batteries in (kW) (on primary *y axis*); SOC [%] (on secondary *y-axis*) (PV and $P_{\mathrm{BATmax}} = 3$kW, SOC$_0$ = SOC$_{24}$=100%). On the *x-axis* the hours of the day and above the peaks count (from 1p to 12p). Signs at time 6 P.M.(18) and 7 P.M. (19) are recalled in Figs. 15 and 16.

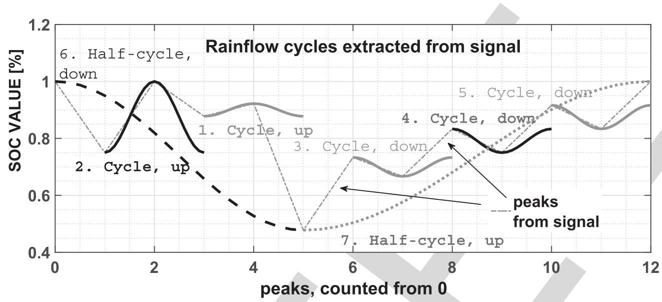

Fig. 11. Scenario n.2: identification and counting of cycles to failure. On the *y*-axis the SOC in % (the dotted of Fig. 10 and the superimposed peak identification and associated cycle or half-cycle) on the *x*-axis the peaks count.

because a single generator can be used at any given time, leaving the second one as backup.

The BESS power and SOC are shown in Figs. 9 and 10, it can be noted that the optimal starting SOC is different (in Scenario n.1 is 40%, while in Scenario n.2 is 100%). The Rainflow counting method is applied to the SOC of Scenario n.2 of Fig. 10 (on the *x*-axis one can read both the time of the day and the counting of peaks and valleys, pointed by the downward arrows) and shown in Fig. 11 for the 12 major trends (up and down) deducted from the scenario itself. The changes in the level of the storage is resolved in individual cycles, in a given interval, and used within the model of *cycles to failure* to cumulatively estimate the battery wearing out. Note that the dotted line in Fig. 11 is the SOC curve from Fig. 10, on top of which the cycles to

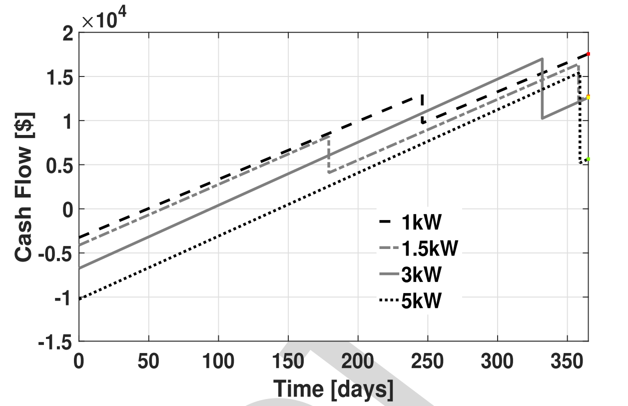

Fig. 12. Scenario n.2 (with PV=3kW$_P$): Economic evaluation on 365 days: on the *y-axis* the Cash flow in [$], on the *x-axis* the considered horizon [in days] for the four investigated battery sizes, investment costs from Table II and fuel cost 3.964 $/gal.

failure for the batteries are counted. The results of the Rainflow counting method are combined with the battery data in Fig. 4 to create the cost analysis curves in Fig. 12, where the cash flow of four different BESS sizes (1, 1.5, 3 and 5 kW) are plotted versus the total number of days (the set horizon). We verified and compared how the investment, which depends on the BESS size, is compensated by the saving in fuel over a set horizon, according to

$$G(\text{size, horizon}) = -\text{Inv(size)} + N_F(\text{size}) \cdot C_{\text{fuel}} \cdot \Delta\text{fuel(size, horizon)} \quad (11)$$

where G the *Gain* is the cash flow in \$, Inv is the investment in \$, N_F the days to failure of the batteries (depending on the number and DoD of the counted cycles), C_{fuel} is the specific fuel cost (\$ /gal) and Δfuel is the daily difference between consumption due to the traditional management of the diesel generators of [2] against the optimized one (in gal/day). In this example, a 365-days horizon is implemented and the 1 kW BESS is identified as the most cost effective configuration because it yields the greatest cash flow at the end of the year. It is worth noting that if the FOB needs to be operative for less than 365 days, for example, in the range between 240 and 300 days, then the 3kW size BESS achieves the highest cash flow and should be used.

B. Experimental Set Up and Verification

The objective of this section is to demonstrate how the OEMS hardware executes the commands sent by the optimized secondary controller presented in the previous sections. A scaled laboratory prototype was built and tested that responds to the four different commands.

1) While the genset is ON, switch from drawing additional power from the battery bank to battery charging mode.
2) While the genset is ON, switch from battery charging mode to drawing additional power from the battery bank.
3) Turnoff the genset and transition to battery-only power mode.

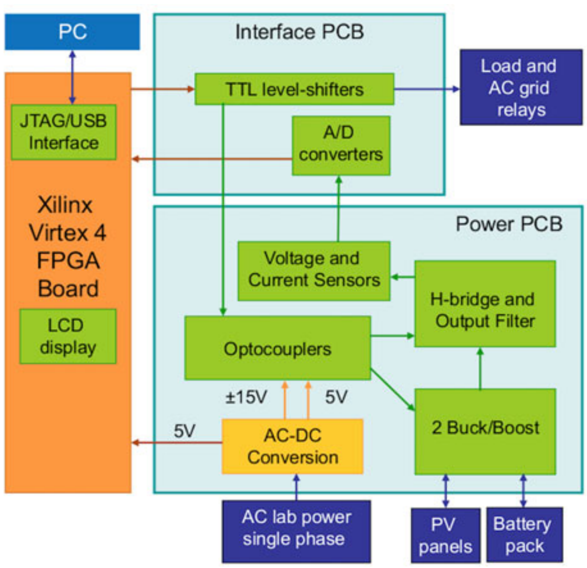

Fig. 13. OEMS hardware block diagram.

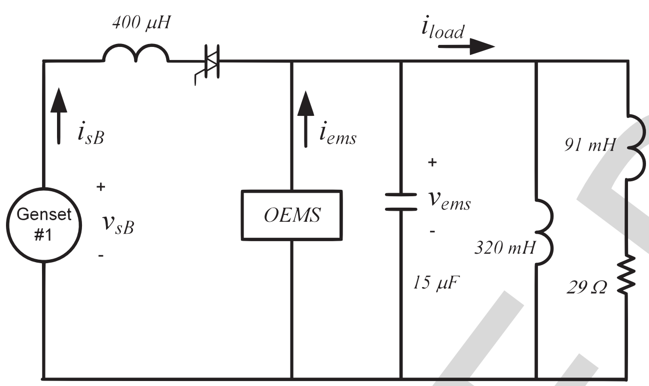

Fig. 14. Laboratory setup.

4) Transition from battery-only power mode to the generator powering the load after the genset is turned ON.

The OEMS' secondary controller is responsible for such commands in either of the two scenarios, with some clarifications following below. The OEMS laboratory prototype includes an FPGA development board, a power PCB, and an interface PCB as shown in Fig. 13.

The OEMS power circuit is shown in Fig. 1 and further details of the hardware implementation and control system can be found in [15]. The circuit shown in Fig. 14 was assembled in the laboratory to demonstrate how the OEMS hardware responds to the secondary controller's commands. The diesel generator Genset #1 was simulated by the ac grid, which provides a 120 V rms voltage source, just like a diesel generator would. The power level of the experiment is a few hundred watts as the main goal is to demonstrate the hardware functionality, not its power rating. The dc bus (shown in Fig. 1) was regulated at 200 V and lead acid batteries were used for the energy storage element.

The voltage and current waveforms demonstrating the execution of the first command of the above list are displayed in Fig. 15. The load is initially powered by the generator and the battery together. At $t = 0$, the OEMS reverses the power flow

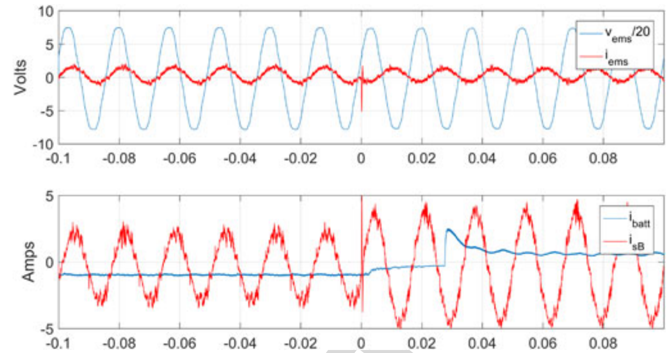

Fig. 15. Transition from drawing additional power from the battery bank to battery charging mode. The generator is kept on (see Scenario n.2 at time 7 P.M. (19:00), small spirals).

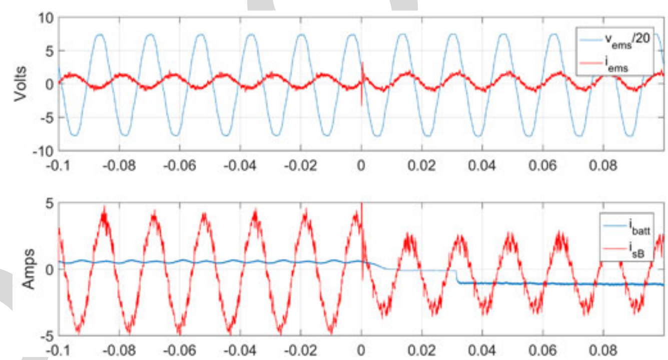

Fig. 16. Transition from battery charging mode to drawing additional power from the battery bank. The generator is kept on (see Scenario n.2 at time 6 P.M. (18:00), small spirals).

from/to the battery. The power flow reversal from the battery can be easily identified in the top plot of Fig. 15, where the OEMS current i_{ems} has a phase shift of 180° at $t = 0$ when the battery quits providing power to the load and begins charging the battery. The bottom plot in Fig. 15, the dc battery current goes from negative (current out of the battery) to positive (current into the battery) and the generator current increases to support the load and the charging of the battery.

In Fig. 16, the voltage and current waveforms, demonstrating the execution of the second command of the list, are displayed. The power flow reversal is executed by the OEMS in reverse order with respect to the previous experiment shown in Fig. 15. Initially, the generator powers the load and charges the battery, then at $t = 0$ the power flow is reversed and the battery supplements the generator power instead of being charged.

The implementation of the third command of the list is displayed in Fig. 17, where the generator is turned OFF and the power to the load comes only from the battery. Once again the transition is transparent to the load which cannot be disrupted at any time. Note that an example of this transition occurs in Scenario n.1 at 9 AM where the additional turn ON of the 15 kW generator can be observed. In practice, the 15 kW generator does not turn ON at the same instant as the 5 kW generator turns OFF, but a few seconds later.

In Fig. 18, the voltage and current waveforms demonstrating the execution of the fourth command of the list are displayed.

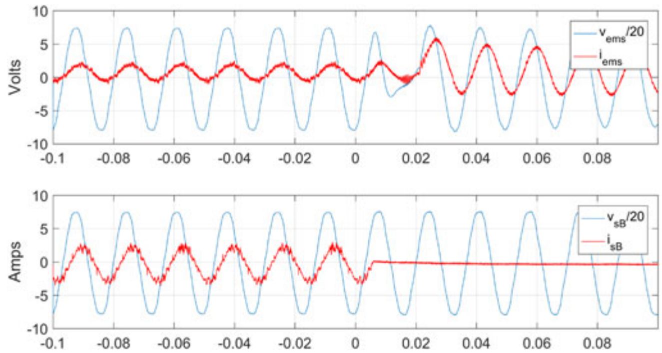

Fig. 17. Disconnect from the generator to transition into battery-only power mode.

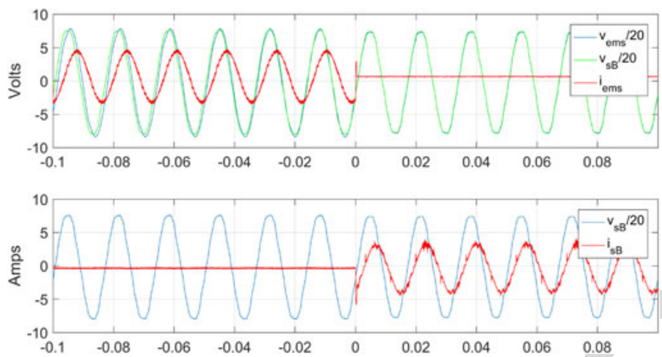

Fig. 18. Step change from battery-only power to battery and generator power after the generator is powered ON.

The load is initially powered only by the battery while the OEMS reduces the phase difference between the generator's voltage and its own. At $t = 0$, the OEMS latches to the generator's voltage and the load becomes powered by the generator while the OEMS current i_{ems} goes to zero. This transition is transparent to the load. Note that although there is not an example of this transition in the analyzed scenarios, this is just the first step necessary to accomplish other transitions, where the battery is subsequently charged from the generator. The complete transition does not occur instantaneously as it appears in Fig. 5 and 6, but in steps that occur within seconds or less.

V. Conclusions and Future Work

This paper presents an OEMS which minimizes the fuel consumption of the diesel generators used in an FOBâĂŹs microgrid, by addressing several questions, among which the best BESS size according to the operating days of the FOB. Furthermore, our formulation and solution have demonstrated that the 80% derating practice, typically used when sizing diesel generators in FOBs, is not necessary, because a single generator can be used at any given time, leaving the second one as backup. A MILP formulation, suitably solved by means of SOS2 and SOS1, has been successfully demonstrated. Its simplicity leads to robustness and ease of implementation. The Rainflow counting method was used to determine the most cost effective BESS size with a given operating time, including a 3 kW$_P$ source. This condition (on given operating times) thus needs to be taken into better account for the future operative planning of the basis.

Two 24-h scenarios were analyzed and showed fuel savings in the range of $30-50\%$ with respect to a previous improved configuration. Such approach provides an estimate of the range of fuel savings, should the PV source fail. The analysis of the two scenarios shows that, as long as the operating days of the FOB are below 240 days or above 300, the best size for the BESS is 1 kW (6 kWh capacity), but if the operating days are between 240 and 300, the 3 kW battery (18 kWh capacity) is the best choice.

A laboratory prototype has been built to demonstrate the OEMS functionality. It has also been demonstrated that the OEMS can carry out the commands produced by the optimization algorithm without disturbing the bus voltage to which critical loads are connected. Future work will analyze the impact of adding supercapacitors to the BESS to further increase the battery's lifetime and to service unexpected load transients of short duration.

References

[1] B. Frazee, "Energy symposium looks at reducing the load in marine corps expeditionary operations," Feb. 2010. [Online]. Available: http://www.marforres.marines.mil/MFRNews/NewsArticleDisplay/tabid/7930/Article/81664/

[2] R. Kelly, G. Oriti, and A. Julian, "Reducing fuel consumption at a remote military base: Introducing an energy management system," *IEEE Electrif. Mag.*, vol. 1, no. 2, pp. 30–37, Dec. 2013.

[3] G. Quartarone, M. Liserre, F. Fuchs, N. Anglani, and G. Buticchi, "Impact of the modularity on the efficiency of smart transformer solutions," 2014, pp. 1512–1518. [Online]. Available: https://www.scopus.com/inward/record.uri?eid=2-s2.0-84983097250&doi=10.1109%2fIECON.2014 7048702&partnerID=40&md5=f0f30c6dc2c06379b4f901132e6fb6a2

[4] N. Anglani, G. Oriti, and M. Colombini, "Optimized energy management system to reduce fuel consumption in remote military microgrids," in *Proc. IEEE Energy Convers. Congr. Expo.*, Sep. 2016, pp. 1–8.

[5] C. Hernandez-Aramburo, T. Green, and N. Mugniot, "Fuel consumption minimization of a microgrid," *IEEE Trans. Ind. Appl*, vol. 41, no. 3, pp. 673–681, May 2005.

[6] F. Mohamed and H. Koivo, "System modelling and online optimal management of microgrid using multiobjective optimization," in *Proc. Int. Conf. Clean Elect. Power*, May 2007, pp. 148–153.

[7] C. Chen, S. Duan, T. Cai, B. Liu, and G. Hu, "Optimal allocation and economic analysis of energy storage system in microgrids," *IEEE Trans. Power Electron.*, vol. 26, no. 10, pp. 2762–2773, Oct. 2011.

[8] Q. Fu *et al.*, "Microgrid generation capacity design with renewables and energy storage addressing power quality and surety," *IEEE Trans. Smart Grid*, vol. 3, no. 4, pp. 2019–2027, Dec. 2012.

[9] W. Zhang, F. Lee, and P.-Y. Huang, "Energy management system control and experiment for future home," in *Proc. IEEE Energy Convers. Congr. Expo.*, Sep. 2014, pp. 3317–3324.

[10] F. Berthold, B. Blunier, D. Bouquain, S. Williamson, and A. Miraoui, "Offline and online optimization of plug-in hybrid electric vehicle energy usage (home-to-vehicle and vehicle-to-home)," in *Proc. IEEE Transp. Electrif. Conf. Expo.*, Jun. 2012, pp. 1–6.

[11] F. Fattori, N. Anglani, and G. Muliere, "Combining photovoltaic energy with electric vehicles, smart charging and vehicle-to-grid," *Solar Energy*, vol. 110, pp. 438–451, 2014. [Online]. Available: http://www.sciencedirect.com/science/article/pii/S0038092X14004745

[12] E. Camponogara, K. Campos de Almeida, and R. Hardt, "Piecewise-linear approximations for a non-linear transmission expansion planning problem," *IET Gener. Transm. Distrib.*, vol. 9, no. 12, pp. 1235–1244, 2015.

[13] M. Tankari, M. Camara, B. Dakyo, and G. Lefebvre, "Use of ultracapacitors and batteries for efficient energy management in wind-diesel hybrid system," *IEEE Trans. Sustain. Energy*, vol. 4, no. 2, pp. 414–424, Apr. 2013.

[14] S. Booth and S. Booth, *Net Zero Energy Military Installations: A Guide to Assessment and Planning*. National Renewable Energy Laboratory, Golden, CO, USA, 2010.

[15] G. Oriti, A. Julian, and N. Peck, "Power-electronics-based energy management system with storage," *IEEE Trans. Power Electron.*, vol. 31, no. 1, pp. 452–460, Jan. 2016.

[16] 2016. [Online]. Available: http://www.africapowersystems.com/

[17] 2017. [Online]. Available: https://powersuite.cummins.com/PSWEB/login.action

[18] 2017. [Online]. Available: http://www.sdmo.com/EN/Products/PPR/Power-gen-products

[19] C. Cho, J.-H. Jeon, J.-Y. Kim, S. Kwon, K. Park, and S. Kim, "Active synchronizing control of a microgrid," *IEEE Trans. Power Electron.*, vol. 26, no. 12, pp. 3707–3719, Dec. 2011.

[20] 2016. [Online]. Available: http://lpsolve.sourceforge.net/

[21] E. Beale and J. Forrest, "Global optimization using special ordered sets," *Math. Program.*, vol. 10, pp. 52–69, 1976.

[22] J. Tomlin, "Special ordered sets and an application to gas supply operations planning," *Math. Program.*, vol. 42, pp 69–84, 1988.

[23] M. Miner, "Cumulative damage in fatigue," *J. Appl. Mech.*, 1945. [Online]. Available: http://scholar.google.it/scholar?q=miner+fatigue&btnG=&hl=it&as_sdt =0,5#0

[24] W. Facinelli, "Modeling and simulation of lead-acid batteries for photovoltaic systems," 1983. [Online]. Available: http://scholar.google.it/scholar?q=facinelli+battery&hl=it&as_sdt=0, 5#3

[25] J. Manwell, J. McGowan, W. Stein, and A. Rogers, "Developments in experimental simulation of wind/diesel systems," *Proc. EWEC 1989*, 1989. [Online]. Available: http://scholar.google.it/scholar?q=rogers+wind/diesel&btnG=&hl=it&as _sdt=0,5#3

[26] J. Collins, *Failure of Materials in Mechanical Design, 1981*. Wiley, New York, NY, USA, 1981. [Online]. Available: http://scholar.google.it/scholar?q=Failure+of+Materials+in+Design.+collins+1981&btnG=&hl=it&as_sdt=0,5#0

[27] R. Dufo-López and J. L. Bernal-Agust ín, "Multi-objective design of PV–wind–diesel–hydrogen–battery systems," *Renew. Energy*, vol. 33, no. 12, pp. 2559–2572, Dec. 2008.

[28] R. Dufo-López *et al.*, "Multi-objective optimization minimizing cost and life cycle emissions of stand-alone PV–wind–diesel systems with batteries storage," *Appl. Energy*, vol. 88, no. 11, pp. 4033–4041, Nov. 2011.

[29] 2017. "Genesis 150 np12-12 batteries—specifications," [Online]. Available: http://datasheet.octopart.com/NP12–12-EnerSys-datasheet-10655.pdf

[30] S. Downing and D. Socie, "Simple rainflow counting algorithms," *Int. J. Fatigue*, vol. 4, no. 1, pp. 31–40, Jan. 1982. [Online]. Available: http://www.sciencedirect.com/science/article/pii/0142112382900184

[31] A. Nieslony, "MATLAB central-rainflow counting algorithm," 2010. [Online]. Available: http://scholar.google.it/scholar?hl=it&q=adam+nieslony+Rainflow+Counti ng+Algorithm&btnG=&lr=#2

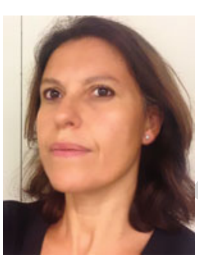

Norma Anglani (S'93–M'99) received the Laurea (with Hons.) and Ph.D. degrees in electrical engineering from the University of Pavia, Pavia, Italy, in 1993 and 1999, respectively.

After graduating, she worked for a consulting company in the energy efficiency area. She was a Postdoctoral Fellow in the Energy Analysis Group with the Energy Efficiency Standards Group, Lawrence Berkeley National Laboratory, Berkeley, CA, USA. She is currently an Assistant Professor with the Department of Electrical, Computer, and Biomedical Engineering, University of Pavia (I), Pavia, where she currently teaches and does research in the field of energy management, energy planning, modeling, and efficient compressed air systems. There, she set up the Labac Laboratory, University of Pavia, a joint effort between academia and industry. She has been responsible for several research contracts with public and private bodies, and has co-authored more than 60 scientific papers.

Dr. Anglani has been a Chartered Engineer since 1995.

Giovanna Oriti (S'94–M'97–SM'04) received the Laurea (with Hons.) and Ph.D. degrees in electrical engineering from the University of Catania, Catania, Italy, in 1993 and 1997, respectively.

She was a Research Intern at the University of Wisconsin, Madison, WI, USA, for two years. After graduation, she joined the United Technology Research Center, East Hartford, CT, USA, where she developed innovative power converter topologies and control. In 2000, she launched her own consulting business developing physics-based models of power converters and drives for electromagnetic interference analysis, stability analysis, and development of control algorithms. In April 2008, she joined the faculty of the Electrical and Computer Engineering Department, Naval Postgraduate School, Monterey, CA, USA, where she is currently an Associate Professor. Her research interests include power electronics for energy management, microgrids, and renewable energy interface. She holds one U.S. Patent and has co-authored more than 40 papers published in IEEE TRANSACTIONS or IEEE Conference Proceedings.

Dr. Oriti served as the Chair of the Industrial Power Conversion System Department, IEEE Industry Application Society (IAS), in 2011–2012. She received the 2002 IEEE IAS Outstanding Young Member Award. In 2012, she received the Electrical and Computer Engineering (ECE) Department, Naval Postgraduate School (NPS) Service Award in recognition of her contribution to the development of the new NPS Electrical Engineering Energy curriculum. In 2016, she received the NPS ECE Research Award in recognition of her contribution, through her research, to the U.S. Navy's goal of energy efficiency.

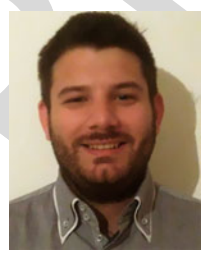

Michele Colombini received the Laurea degree in electrical engineering from the University of Pavia, Pavia, Italy, in 2014.

He received a research scholarship for six months to study the technical and economic feasibility of middle-sized steam screw expanders for energy-intensive industrial facilities, such as the paper industry. Since September 2015, he has been with Generac Mobile Products SRL, Villanova d'Ardenghi, Italy, a Generac Power System, Inc. subsidiary, specializing in tower light production. He is currently with the Research and Development Department to develop a new hybrid-fed tower light system, where he is in charge of the simulations for the assessment of the fuel savings due to innovative-fed systems.

Optimized Energy Management System to Reduce Fuel Consumption in Remote Military Microgrids

Norma Anglani, Giovanna Oriti, and Michele Colombini

***Abstract*—This paper presents an optimized energy management system (OEMS) to control the microgrid of a remote temporary military base (FOB) featuring diesel generators, a battery energy storage system (BESS), and photovoltaic (PV) panels. The information of the expected electric demand is suitably used to improve the sizing and management of the BESS, according to the days of operation. The OEMS includes power electronics to charge the batteries from either the PV source or the diesel generators, and it can function as a current source when it is supplementing the power from one of the generators or as a voltage source when it is the sole source of power for the loads. The new contribution of this paper includes the optimization of a FOB's microgrid, where critical loads must be serviced at all times. The proposed optimization, which uses Special Order Sets for the semicontinuous function handling, also integrates economic evaluations by properly taking into account how the size of BESS affects its charge/discharge cycle; thus, the FOBs' battery lifetime, in addition to its fuel consumption. Results from optimization are employed by the OEMS to coordinate the energy sources, and match the critical and noncritical loads with the available supply. Fuel savings of $\approx 30\%$ (and $\approx 50\%$ adding the PV source) can be achieved with respect to the already improved, but not optimal, solution of a previous work.**

***Index Terms*—Energy management system (EMS), microgrid, mixed integer linear optimization (MILP), rain flow counting method, renewables integration, Special Ordered Set (SOS).**

I. Introduction

RECENT emphasis on energy efficiency has stimulated the use of smart hybrid power supply systems in remote military camps such as the U.S. Marine Corps forward operating bases (FOBs) [1], [2], also in view of new electrifying paradigms [3]. Reducing fuel consumption results both in reduced operational cost for the FOB, and it can also save soldiers' lives because fuel transportation is dangerous, especially outside U.S. borders. Recently developed FOBs' power systems include a battery energy storage system (BESS) and renewable energy sources such as photovoltaic (PV) panels in addition to traditional diesel generators [4]. In [2], a power electronics based energy management system (EMS) was used to significantly reduce fuel consumption in a power system featuring two diesel generators and a BESS; however, the study did not consider the BESS state of charge (SOC), lifetime, cost, or the addition of PV sources recently introduced in FOBs. In this paper, an optimized EMS (OEMS) is presented where a simple but robust algorithm manages the diesel generators, the BESS, and PV source as shown in Fig. 1.

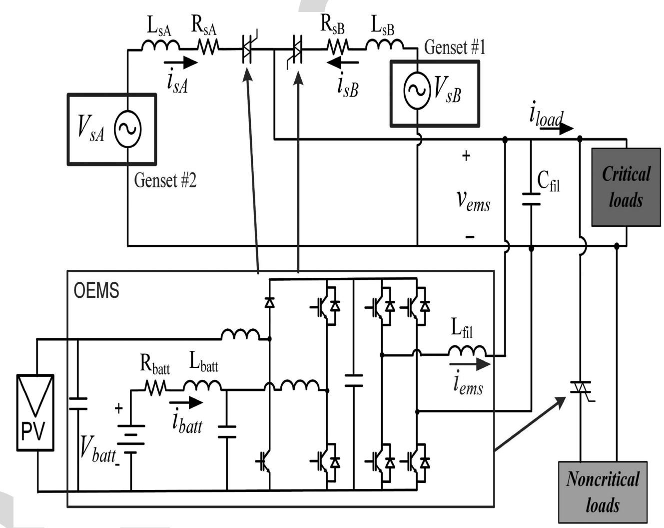

Fig. 1. Optimized energy management system architecture.

Critical loads in the schematic are those electrical devices that must be powered at all times to ensure the success of the military operation. The optimization strategy includes lifetime and economic considerations for the BESS; thus, managing the cost of the microgrid while reducing fuel consumption. Applications of online and offline optimization techniques in the management of energy supply and demand are widely available as in [5], [6], and [7] and more recently in [8] and [9]. They are applied not only to microgrids, as in [10], but also to assess the impact on bigger energy system, as in [11]. Although some of these papers deal with critical load service and fuel consumption, none of them addresses remote military microgrids and their key issues. In the knowledge of the authors, few examples have been able to achieve such amount of savings, by making the optimization problem as simple as it is shown. Supported by the work of Camponogara *et al.* [12], with respect to the use of the Special

Manuscript received October 28, 2016; revised March 14, 2017 and May 8, 2017; accepted July 7, 2017. Paper 2016-SECSC-1156.R2, presented at the 2016 IEEE Energy Conversion Congress and Exposition, Milwaukee, WI, USA, Sep. 18–22, and approved for publication in the IEEE Transactions on Industry Applications by the Sustainable Energy Conversion Systems Committee of the IEEE Industry Applications Society. *(Corresponding author: Norma Anglani.)*

N. Anglani is with the University of Pavia, Pavia 27100, Italy (e-mail: nanglani@unipv.it).

G. Oriti is with the Naval Postgraduate School, Monterey, CA 93943 USA (e-mail: goriti@nps.edu).

M. Colombini is with the Generac Mobile Product srl, Villanova d'Ardenghi 27030, Italy (e-mail: mich.colombini@gmail.com).

Color versions of one or more of the figures in this paper are available online at http://ieeexplore.ieee.org.

Digital Object Identifier 10.1109/TIA.2017.2734045

Ordered Sets (SOSs) and by the work of Tankari *et al.* (2013) in the use of the rainflow counting method [13], we tailored the algorithms and match them together to find a solution to the problem of minimizing the fuel consumptions of the FOBs and optimize the BESS size, according to the operating days. No previous work solved the specific problems of a FOB, except [14], which proposes the use of HOMER, but with different purposes. In this paper, a well-known mixed integer linear programming (MILP) formulation is proposed for the OEMS. Although MILP is less sophisticated than other algorithms available in the literature, analysis shows that its robustness is a fundamental asset to speed up controlling strategies and obtain satisfactory results.

The new contribution of this paper includes the overall optimization procedure which uses SOSs for the semicontinuous function handling, and integrates economic evaluations by properly taking into account how the size of BESS affects its charge/discharge cycle; thus, the battery lifetime. Another new contribution is the hardware implementation of the optimized control system; in a laboratory prototype the OEMS coordinates the energy sources and BESS to service critical and noncritical loads using the results from the proposed optimization. It should be noted that the application of microgrid technology to FOBs is rarely found in the literature, therefore this paper is also new in the application that it presents. One important variable that must be considered in a FOB is that critical loads must be serviced at all times, even if this results in shedding of noncritical loads when a fault occurs. With the proposed algorithm, we operate to avoid the shedding. Two optimized scenarios, with and without a PV source, demonstrate fuel savings of $\approx 30\% - 50\%$, respectively, compared to previous work [2]. The scenarios approach supports a sensitivity analysis on the amount of savings, when the PV production may fail. Experimental measurements demonstrate the OEMS functionality.

In Section II, the power electronics based OEMS will be illustrated. In Section III, the formulation of the optimization problem, the methodology based on SOS-constraints, and the rainflow counting method are presented to solve the minimization of the fuel consumption and for the optimal sizing of the BESS. The case study and the sizing are described and solved in Section IV, according to the operating days, conclusions are drawn in Section V.

II. Power Electronics Based EMS

The EMS depicted in Fig. 1 includes three inverter legs and a field programmable gate array (FPGA) based control system. Two of the legs are used for a bidirectional H-bridge converter which converts power from the dc bus to the ac loads and vice-versa. The other two legs are used for the battery pack and PV panels, respectively. Since the PV source power flows unidirectionally, only one switch and one diode of the fourth inverter leg are used for the boost converter that conditions the PV power. The EMS includes a primary controller [15] for the power electronics and a secondary controller to manage the loads and distributed resources, including storage and PV. Solid state switches are used to connect and disconnect the two generator sets (gensets) and the noncritical loads, which can be shed if there is a power failure or to control peak power consumption. While Oriti *et al.* [15] focus on the EMS primary control system, this paper focuses on the secondary controller which gives the OEMS the ability to optimally manage loads and the BESS SOC.

III. Problem Formulation: MILP, SOSs, and the Rainflow Counting Method

In the following, we explain how we combine two techniques to provide an optimized secondary control law, able to answer the questions.

1) Which is the best configuration to save fuel and size batteries in a FOB, according to the number of operating days?
2) Which is the range of savings, if PV panels are used?
3) How can we realize it?

At first, we propose a formulation which improves the original setup reported in [2], second, we evolve toward a hybrid microgrid configuration, by adding the new PV plant and finally we optimize the size of the battery according to the economics and the life time of the microgrid (i.e., the operative days of the base). The results of such constrained optimization problem become instrumental for the OEMS described in the previous section. We look at a typical day, divided into *j*th time steps, then we base our model on two vectors of semicontinuous, nonnegative decision variables: $x_{1,j}$ and $x_{2,j}$ the average load factors of genset #1 (P_{1r}=5 kW, rated power) and genset #2 (P_{2r}=15 kW), as defined in (1.5) of Table I.

One interesting feature in our formulation is represented by the choice to also use, as decision variable, the SOC value at the beginning of the day and impose to have the same value at the end of the day. Such choice allows us to take into account the temporal continuity, while representing a typical day. This is a neglected aspect in many papers dealing with optimization on daily profiles, although it is an important one.

Fig. 2 reports the linearized relationships between gensets' consumption (gal/h, 1gal = 3.79 l)) and $x_{i,j}$ (and also power). Data are elaborated from an extensive research on technical datasheets from several manufacturers' websites like Caterpillar [16], Cummins [17], Kohler [18], providing gensets of suitable size for the proposed case study. Although it may seem simple to draw such relationship, a considerable effort is represented by how such data are sought and interpreted from technical datasheets.

We formulate an optimization problem to minimize the fuel consumption of the facility of Fig. 1, that is

$$f(x_{1,j}, x_{2,j}) = \sum_{\substack{1\le i\le 2\\ 1\le j\le J^*}} C_{i,j} = \begin{cases} m_i \cdot x_{i,j} + q_i & \text{when } x_i^m \le x_{i,j} \le x_i^M \\ 0 & \text{when } x_{i,j} = 0 \end{cases} \quad (1)$$

over a J^* horizon, discretized in j time steps. m_i and q_i are the coefficients of the two linear equations in $x_{i,j}$ of the upper Fig. 2. Additional equations describing the working conditions of the diesel gensets and BESS, also with respect to photovoltaic availability, are reported in Table I with a succinct description.

TABLE I
LIST OF VARIABLES, PARAMETERS, AND EQUATIONS DESCRIBING THE PROBLEM CONDITIONS (AT TIME j)

Variable /parameter	Description of var./param. and/or Eq.	Equations	#
$x_{1,j}$ - $x_{2,j}$	dominion of decision variables (i.e., load factors)	$x_1^m \le x_{1,j} \le 1$ or $x_{1,j} = 0$ $x_2^m \le x_{2,j} \le 1$ or $x_{2,j} = 0$	(1.2)
	no syncro condition	$x_{i,j} > 0 \rightarrow x_{k,j} = 0 \quad \forall k \neq i$	(1.3)
$x_{3,j}$	battery load factor dominion	$-1 \le x_{3,j} \le 1$	(1.4)
$P_{i,j}$	power from gen. and from/to BESS at time j (P_{1r}, P_{2r}, P_{BATmax})	$x_{i,j} = \frac{P_{i,j}}{P_{ir}}$	(1.5)
T_{bat}, E_{bat}	time of discharge at rated P_{BATmax} and capacity of BESS	$E_{\text{bat}} = P_{\text{BATmax}} \cdot T_{\text{bat}}$	(1.6)
L_j, $P_{PV,j}$	Load and available PV power	$x_{1,j} \cdot P_{1r} + x_{2,j} \cdot P_{2r}$ $-x_{3,j} \cdot P_{\text{BATmax}} + (P_{PV,j}) = L_j$	(1.7)
SOC_j in %	state of charge	$SOC_j = SOC_{j-1} + x_{3,j} \cdot \frac{j}{T_{\text{bat}}}$	(1.8)
	decision var.	$SOC_0 = SOC_{J^*}$	(1.9)
	dominion	$SOC^m \le SOC_j \le SOC^M$	(1.10)

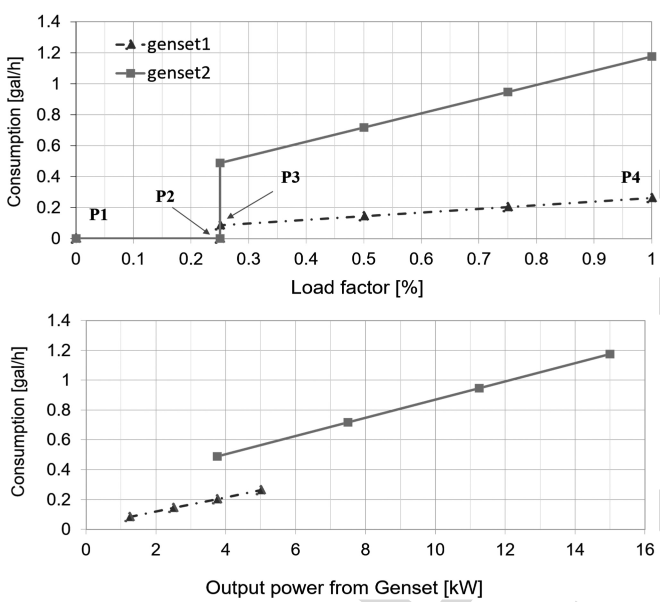

Fig. 2. Fuel consumptions (gal/h) versus load factor (%, or output power in kW) for genset #1 $P_{1,r} = 5$ kW and genset #2 $P_{2,r}$ =15kW. At the top, the coefficients of the linear equations are $m_1 = 0.2366$ - $q_1 = 0.0253$; $m_2 =$ 0.9153. $q_2 = 0.2597$, respectively. Elaboration from [16]–[18].

The constraint, involving $\mathbf{x_3}$ a dependant variable, means that the battery can be charged and discharged (assuming both positive and negative values), having as its hourly limit $\pm P_{\text{BATmax}}$. This condition is set to preserve its lifetime, besides charging and discharging efficiencies are set equal to 1.

In balancing the supply and the demand side, also the contribution of the PV source ($P_{PV,j}$) can be taken into account in a deterministic way, if it exists.

If one of the two diesel generators can be used as a backup power to improve the reliability, no synchronization between the two gensets is required, at this stage [19].

Unfortunately (1) and some constraints in Table I are not straightforwardly applicable to linear programming solvers like CPLEX. The objective function (1) is a sum of the consumption associated with the running of the two gensets

$$\begin{cases} f(x_{1,j}) = 0.2366x_{1,j} + 0.0253 \\ f(x_{2,j}) = 0.9153x_{2,j} + 0.2597 \end{cases} \tag{2}$$

in each time frame jth a new $x_{i,j}$ is assessed. $x_{i,j}$ can either be a value between 0.25 and 1 or be 0, so for each function $f(x_i)$, four major points can be identified by their coordinates: $P_i^1(0,0)$, $P_i^2(0.25^-,0)$, $P_i^3(0.25^+, m_i 0.25 + q_i)$, $P_i^4(1, m_i + q_i)$ (see Fig. 2 where the points are highlighted only for genset #1). Besides, the no synchronization requirement implies that at the time j, $\forall i$

$$x_{i,j} > 0 \Leftrightarrow x_{l,j} = 0 \text{ for } l \neq i. \tag{3}$$

To deal with such features on decision variables, the Special Ordered Sets (SOSs), a tool in the Branch and Bound method to branch groups of variables, are introduced [20]. SOSs of type 2 are functional to deal with piecewise linear continuous functions (like the objective function) and type 1 to deal with the no syncronization requirement as in [21] and [22]. The formulation of a MILP problem is thus given, from the objective function of (1) through the definition of all the conditions expressed in Table I.

A. SOSs Type 2 and Type 1 Resolution

SOS2 is an ordered set of nonnegative variables, where *no more than two adjacent elements can be nonzero* in a feasible solution. Consider $f(y)$, the piecewise linear function in y defined in closed intervals $[\hat{y}_k, \hat{y}_{k+1}]$, where $[\hat{y}_k, f(\hat{y}_k)]$ represent the coordinates of $P_1, ..., P_K$ and $k = 1, ..., K$ (Fig. 3)

y in $[\hat{y}_k, \hat{y}_{k+1}]$ can be written as

$$y = \lambda_k \hat{y}_k + \lambda_{k+1} \hat{y}_{k+1} \tag{4}$$

where

$$\lambda_k + \lambda_{k+1} = 1 \quad \text{and} \quad \lambda_k, \lambda_{k+1} \ge 0. \tag{5}$$

As well, $f(y)$, linear in the interval, can be written as

$$f(y) = \lambda_k f(\hat{y}_k) + \lambda_{k+1} f(\hat{y}_{k+1}) \tag{6}$$

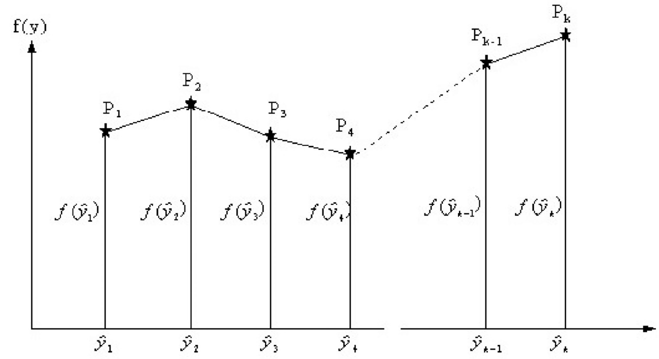

Fig. 3. Generic piecewise linear function $f(y)$ [20].

$f(y)$ can be represented by using a set of *weight* variables λ_k, $k = 1, ..., K$ as

$$f(y) = \lambda_1 f(\hat{y}_1) + \lambda_2 f(\hat{y}_2) + ... + \lambda_K f(\hat{y}_K) \tag{7}$$

where

$$\hat{y}_1\lambda_1 + \hat{y}_2\lambda_2 + ... + \hat{y}_K\lambda_K - y = 0 \qquad y \geq 0 \tag{8}$$

$$\lambda_1 + \lambda_2 + ... + \lambda_K = 1 \qquad \lambda_k \geq 0 \quad k = 1, ..., K. \tag{9}$$

Besides, we must consider the additional condition that no more than two adjacent variable can be nonzero at any time (according to [21] and [22]). These weight variables are the Special Ordered Set type 2.

In an electrical grid, stability is a very important issue as well as redundancy of the supply system: to provide those two requirements for a limited supply system like a FOB can be, where only a few diesel generators exist, we have been assuming that only one generator is running at a time. Taking into account such condition requires the use of SOS1. SOS1 are a set of adjacent subsequent variables where at most one element can be non zero in a feasible solution. Therefore, (9) under the condition of SOS1, that only one element can be nonzero, implies that only one element will be equal to one.

B. Rainflow Counting Method

The addition of batteries and PV sources to a traditional FOB power system leads to fuel savings and CO_2 emission reduction. As the battery size increases the fuel consumption may decrease, but the overall cost of the microgrid will go up. Therefore, battery cost and lifetime must be included in the optimization. In the economic evaluation of a given layout, the real lifetime of a battery is a sensitive parameter depending on the aging, according to the charge/discharge cycles and the DoD (Depth of Discharge). Thus, another step deals with the best sizing of the BESS, according to the typical daily working cycles. The chosen approach was an adaptation of the Miner's Rule [23], introduced by Facinelli in [24]: in brief, he observed that the higher the DoD the lower the lifetime of a battery (see Fig. 4).

Such rule is valid as long as the cycles do not overlap, which is typical of a simple PV+BESS configuration. When the cycles are more irregular, then the rule can not be applied as it is. For instance, this irregularity has been first found in modeling wind/diesel kind of systems [25]. If overlapping and irregular cycles occur, the Rainflow Count, deriving from the original work of Collins [26], later resumed by [27], [28], and [13], can be used.

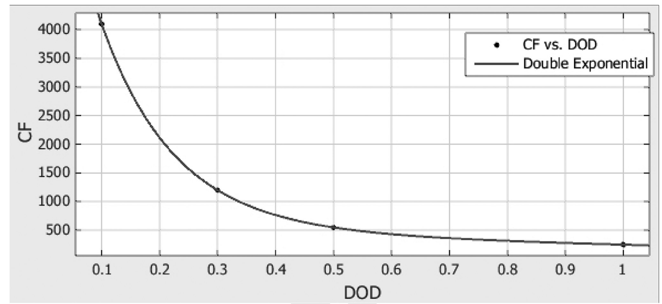

Fig. 4. Fitting curve C_F representing the cycles to failure (lifetime) of batteries versus the fractional DoD, according to data in Table II.

TABLE II
NUMBER OF CYCLES VERSUS DOD FOR LEAD–ACID BATTERIES [29]

Depth of Discharge	# cycle (approx.)
100%	250
50%	550
30%	1200
10%	4100

Investment Costs: $1kW = 3250\$$; 1.5 kW = 4125\$; $3kW = 6750\$$; 5 kW=10250\$

The modeling of the wearing out of batteries due to the cycles of charge/discharge is based on considering the lifetime (cycles to failure) depending on the DoD. According to the details in Table II, the fitting curve is identified and drawn in Fig. 4.

The life fraction is $1/C_F$, if after a given number of cycles the sum of the number of the cycles (N_i) multiplied by the life fraction is greater than 1, then the battery is considered being dead. In other words, the fractional damage *D*, defined as

$$D = \sum_{i=1}^{m} \frac{N_i}{C_{F,i}} \tag{10}$$

is the inverse of the lifetime. The unit of measure depends on how the time horizon cycles are counted: if the DoD cycles are evaluated on a single day, then the lifetime of the battery is counted in days. The lead–acid battery characteristics of Section IV are from [29] and are reported in Table II, along with some costs, useful in the case study.

The technique is based on the work of Downing *et al.* [30] and uses an algorithm created by Nielsony in MatLab code [31], where individual cycles and the range of cycles of batteries are assessed according to what is detailed in Section IV. Although the method is conceptually reasonable and it consists of the separation of cycles it must be pointed out that there is no experimental validation of it.

IV. RESULTS FOR THE CASE STUDY OF A FOB

This section demonstrates that the optimized algorithm embedded in the OEMS' secondary controller reduces the overall

TABLE III
RELEVANT INPUT AND OUTPUT DATA FOR BOTH THE SCENARIOS (ON A TYPICAL DAY $J^* = 24$)

Description input	Scenario n.1 (no PV)	Scenario n.2 (with PV)
$x_{1,j}$ - $x_{2,j}$	0 or 0.25 ÷ 1 (semicont.)	0 or 0.25 ÷ 1 (semicont.)
$x_{3,j}$	−1 ÷ 1	−1 ÷ 1
P_{1r}-P_{2r}-P_{BATmax} in kW	5 − 15 − 3	5 − 15 − 3
T_{bat} in h (@ $P_{\text{BATmax}} = 3kW_P$)	6	6
SOC^m-SOC^M in $kWh(and\%)$	3.6–18 (20%–100%)	3.6–18 (20%–100%)
P_{PV} peak power in kW	0	3
output		
$SOC_0 = SOC_{24}$ in %	40%	100% (see Figs. 9 and 10)
Consump. in gal/day (savings in %)	7.7 (31%)	4.65 (58%) (see Figs. 7 and 8)

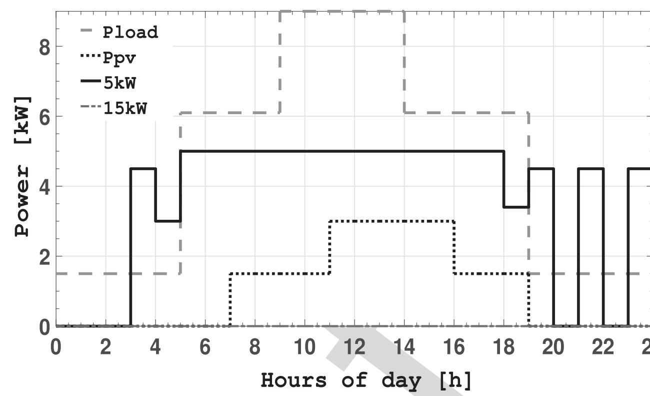

Fig. 6. Scenario n.2: Load and Power from generators (PV and P_{BATmax} both equal to 3kW, $\text{SOC}_0 = \text{SOC}_{24}$).

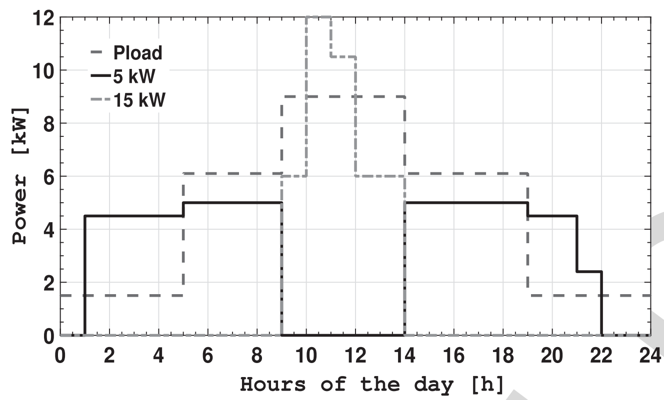

Fig. 5. Scenario n.1: Load and Power from generators (P_{BATmax} equal to 3 kW, $\text{SOC}_0 = \text{SOC}_{24}$, no PV).

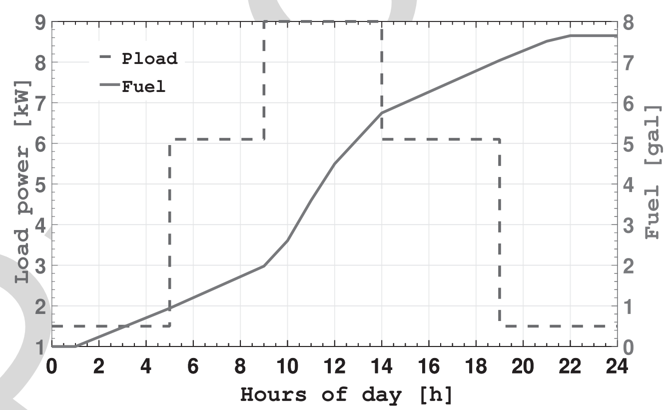

Fig. 7. Scenario n.1: Load and Consumption, power in (kW) on the primary *y-axis*, consumption in (gal) on the secondary *y-axis* (P_{BATmax} equal to 3kW, $\text{SOC}_0 = \text{SOC}_{24}$, no PV).

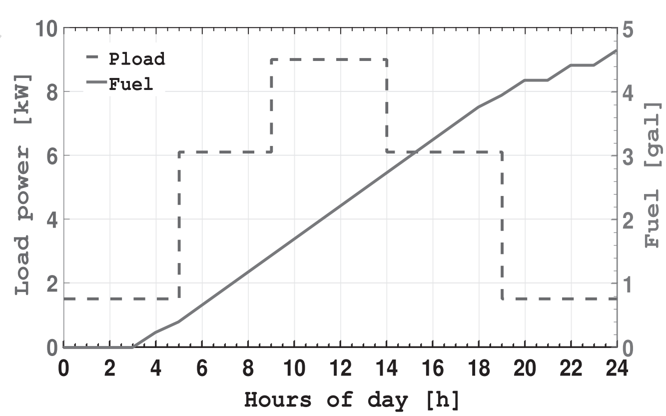

Fig. 8. Scenario n.2: Load and Consumption, power in (kW) on the primary *y-axis*, consumption in (gal) on the secondary *y-axis* (PV and P_{BATmax} both equal to 3kW, $\text{SOC}_0 = \text{SOC}_{24}$).

cost of the microgrid by including battery lifetime expectation and a load management algorithm, more sophisticated than the one presented in [2]. The experimental results are also illustrated.

A. Optimization and Cost Analysis: The Two Scenarios

In Table III, the most relevant input data are listed for two scenarios: the first without a PV panel, to compare results with the analysis in [2], the second with a 3 kW$_P$ PV panel. At the bottom of Table III, the most important outcomes from the optimization are reported: the optimal initial SOC, the consumption (gal/h), and the savings (%) against the original configuration, where 11.2 gal/day (42.4 l/day) were consumed with the same set of electrical loads [2]. We use two scenarios also to perform a sensitivity analysis and to report a range of savings in case the PV panels work or not.

The results of the two scenarios are reported in details from Figs. 5 to 10. Figs. 5 and 6 show the power curves over a 24 h period for the load, for the two gensets and for the PV source (only in Scenario n.2). In Scenario n.1, both gensets are used but never at the same time; in Scenario n.2, the OEMS chooses to use only genset #1, leaving genset #2 off. This is the result of the optimization algorithm matching the loads to the sources to minimize fuel consumption, with the addition on security of supply. The fuel consumption over the 24 h period is plotted in Figs. 7 and 8. The total consumed fuel is 7.7 (29.15 l) and 4.65 gallons (17.6 l), which demonstrates in both cases a 31% and 58% reduction, compared to the analysis in [2]. These results demonstrate that the 80% derating practice, typically used when sizing diesel generators in FOBs, is not necessary,

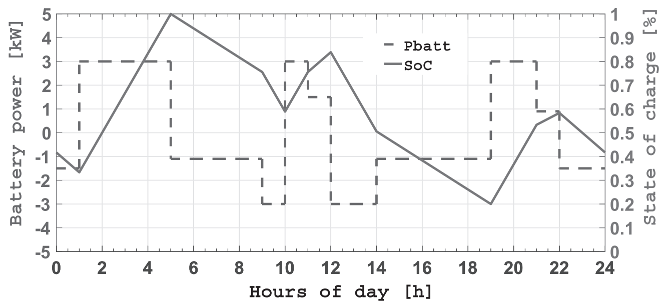

Fig. 9. Scenario n.1: Power from/to Batteries in (kW) (on primary *y-axis*); SOC [%] (on secondary *y-axis*) ($P_{\text{BATmax}} = 3$kW, $\text{SOC}_0{=}\text{SOC}_{24}$, no PV). On the *x-axis* the hours of the typical day.

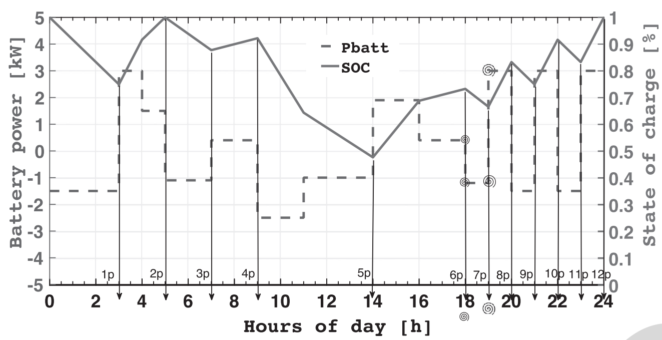

Fig. 10. Scenario n.2: Power from/to Batteries in (kW) (on primary *y axis*); SOC [%] (on secondary *y-axis*) (PV and $P_{\text{BATmax}} = 3$kW, $\text{SOC}_0 = \text{SOC}_{24}{=}100\%$). On the *x-axis* the hours of the day and above the peaks count (from 1p to 12p). Signs at time 6 P.M.(18) and 7 P.M. (19) are recalled in Figs. 15 and 16.

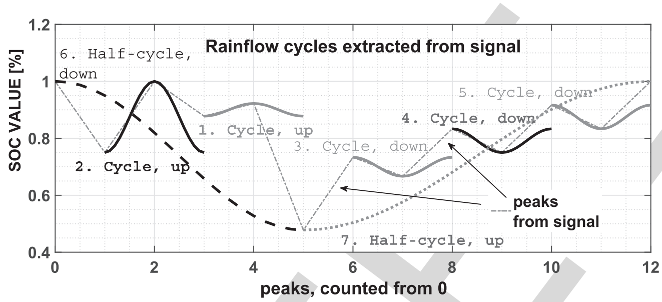

Fig. 11. Scenario n.2: identification and counting of cycles to failure. On the *y*-axis the SOC in % (the dotted of Fig. 10 and the superimposed peak identification and associated cycle or half-cycle) on the *x*-axis the peaks count.

because a single generator can be used at any given time, leaving the second one as backup.

The BESS power and SOC are shown in Figs. 9 and 10, it can be noted that the optimal starting SOC is different (in Scenario n.1 is 40%, while in Scenario n.2 is 100%). The Rainflow counting method is applied to the SOC of Scenario n.2 of Fig. 10 (on the *x*-axis one can read both the time of the day and the counting of peaks and valleys, pointed by the downward arrows) and shown in Fig. 11 for the 12 major trends (up and down) deducted from the scenario itself. The changes in the level of the storage is resolved in individual cycles, in a given interval, and used within the model of *cycles to failure* to cumulatively estimate the battery wearing out. Note that the dotted line in Fig. 11 is the SOC curve from Fig. 10, on top of which the cycles to

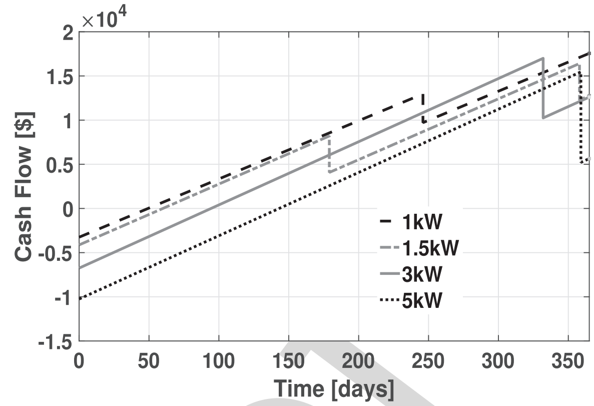

Fig. 12. Scenario n.2 (with PV=3kW$_P$): Economic evaluation on 365 days: on the *y-axis* the Cash flow in [$], on the *x-axis* the considered horizon [in days] for the four investigated battery sizes, investment costs from Table II and fuel cost 3.964 $/gal.

failure for the batteries are counted. The results of the Rainflow counting method are combined with the battery data in Fig. 4 to create the cost analysis curves in Fig. 12, where the cash flow of four different BESS sizes (1, 1.5, 3 and 5 kW) are plotted versus the total number of days (the set horizon). We verified and compared how the investment, which depends on the BESS size, is compensated by the saving in fuel over a set horizon, according to

$$G(\text{size, horizon}) = -\text{Inv(size)} + N_F\,(\text{size}) \cdot C_{\text{fuel}} \cdot \Delta\text{fuel(size, horizon)} \tag{11}$$

where G the *Gain* is the cash flow in \$, Inv is the investment in \$, N_F the days to failure of the batteries (depending on the number and DoD of the counted cycles), C_{fuel} is the specific fuel cost (\$ /gal) and Δfuel is the daily difference between consumption due to the traditional management of the diesel generators of [2] against the optimized one (in gal/day). In this example, a 365-days horizon is implemented and the 1 kW BESS is identified as the most cost effective configuration because it yields the greatest cash flow at the end of the year. It is worth noting that if the FOB needs to be operative for less than 365 days, for example, in the range between 240 and 300 days, then the 3kW size BESS achieves the highest cash flow and should be used.

B. Experimental Set Up and Verification

The objective of this section is to demonstrate how the OEMS hardware executes the commands sent by the optimized secondary controller presented in the previous sections. A scaled laboratory prototype was built and tested that responds to the four different commands.

1) While the genset is ON, switch from drawing additional power from the battery bank to battery charging mode.
2) While the genset is ON, switch from battery charging mode to drawing additional power from the battery bank.
3) Turnoff the genset and transition to battery-only power mode.

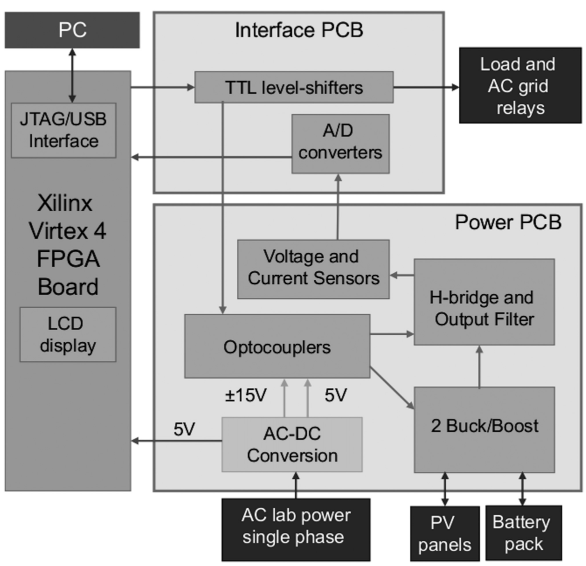

Fig. 13. OEMS hardware block diagram.

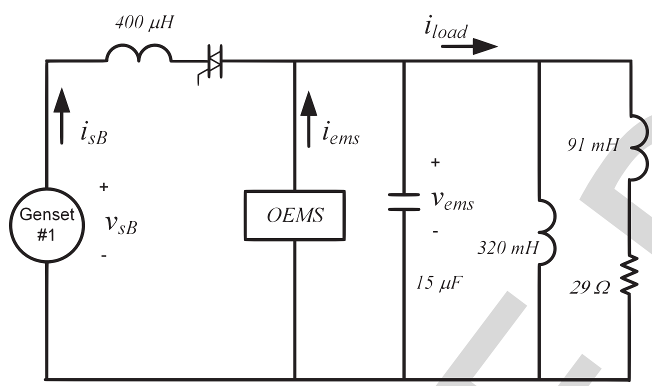

Fig. 14. Laboratory setup.

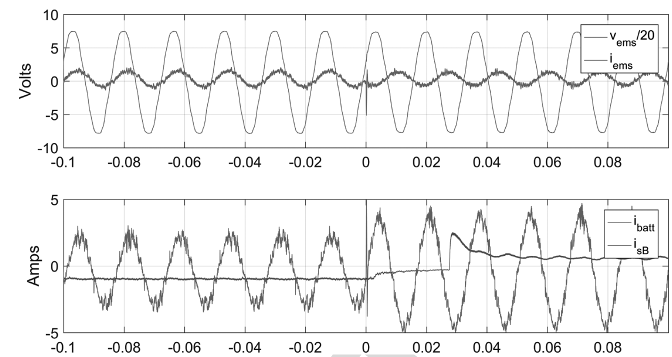

Fig. 15. Transition from drawing additional power from the battery bank to battery charging mode. The generator is kept on (see Scenario n.2 at time 7 P.M. (19:00), small spirals).

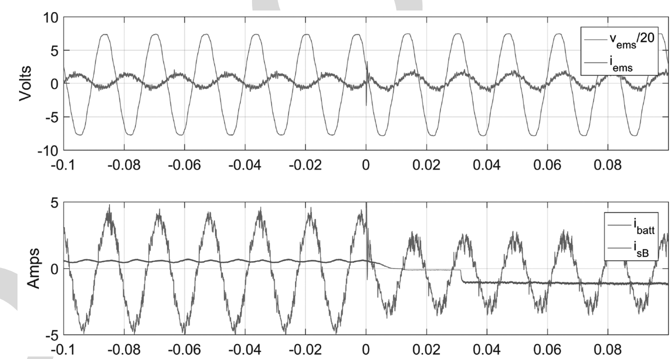

Fig. 16. Transition from battery charging mode to drawing additional power from the battery bank. The generator is kept on (see Scenario n.2 at time 6 P.M. (18:00), small spirals).

4) Transition from battery-only power mode to the generator powering the load after the genset is turned ON.

The OEMS' secondary controller is responsible for such commands in either of the two scenarios, with some clarifications following below. The OEMS laboratory prototype includes an FPGA development board, a power PCB, and an interface PCB as shown in Fig. 13.

The OEMS power circuit is shown in Fig. 1 and further details of the hardware implementation and control system can be found in [15]. The circuit shown in Fig. 14 was assembled in the laboratory to demonstrate how the OEMS hardware responds to the secondary controller's commands. The diesel generator Genset #1 was simulated by the ac grid, which provides a 120 V rms voltage source, just like a diesel generator would. The power level of the experiment is a few hundred watts as the main goal is to demonstrate the hardware functionality, not its power rating. The dc bus (shown in Fig. 1) was regulated at 200 V and lead acid batteries were used for the energy storage element.

The voltage and current waveforms demonstrating the execution of the first command of the above list are displayed in Fig. 15. The load is initially powered by the generator and the battery together. At $t = 0$, the OEMS reverses the power flow from/to the battery. The power flow reversal from the battery can be easily identified in the top plot of Fig. 15, where the OEMS current i_{ems} has a phase shift of 180° at $t = 0$ when the battery quits providing power to the load and begins charging the battery. The bottom plot in Fig. 15, the dc battery current goes from negative (current out of the battery) to positive (current into the battery) and the generator current increases to support the load and the charging of the battery.

In Fig. 16, the voltage and current waveforms, demonstrating the execution of the second command of the list, are displayed. The power flow reversal is executed by the OEMS in reverse order with respect to the previous experiment shown in Fig. 15. Initially, the generator powers the load and charges the battery, then at $t = 0$ the power flow is reversed and the battery supplements the generator power instead of being charged.

The implementation of the third command of the list is displayed in Fig. 17, where the generator is turned OFF and the power to the load comes only from the battery. Once again the transition is transparent to the load which cannot be disrupted at any time. Note that an example of this transition occurs in Scenario n.1 at 9 AM where the additional turn ON of the 15 kW generator can be observed. In practice, the 15 kW generator does not turn ON at the same instant as the 5 kW generator turns OFF, but a few seconds later.

In Fig. 18, the voltage and current waveforms demonstrating the execution of the fourth command of the list are displayed.

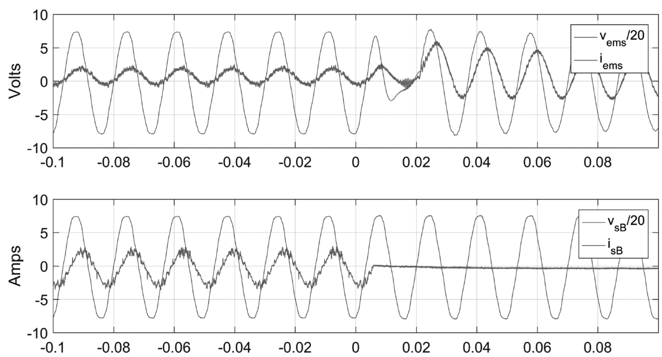

Fig. 17. Disconnect from the generator to transition into battery-only power mode.

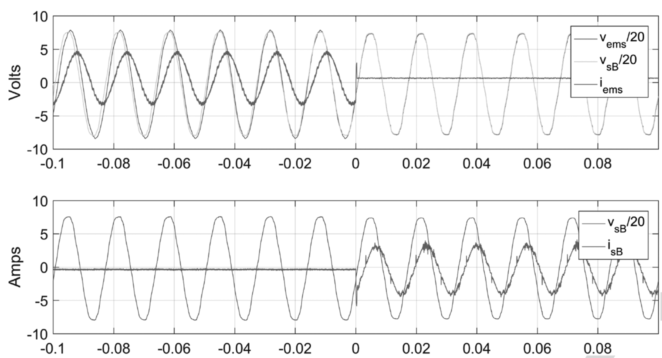

Fig. 18. Step change from battery-only power to battery and generator power after the generator is powered ON.

The load is initially powered only by the battery while the OEMS reduces the phase difference between the generator's voltage and its own. At $t = 0$, the OEMS latches to the generator's voltage and the load becomes powered by the generator while the OEMS current i_{ems} goes to zero. This transition is transparent to the load. Note that although there is not an example of this transition in the analyzed scenarios, this is just the first step necessary to accomplish other transitions, where the battery is subsequently charged from the generator. The complete transition does not occur instantaneously as it appears in Fig. 5 and 6, but in steps that occur within seconds or less.

V. Conclusions and Future Work

This paper presents an OEMS which minimizes the fuel consumption of the diesel generators used in an FOBâĂŹs microgrid, by addressing several questions, among which the best BESS size according to the operating days of the FOB. Furthermore, our formulation and solution have demonstrated that the 80% derating practice, typically used when sizing diesel generators in FOBs, is not necessary, because a single generator can be used at any given time, leaving the second one as backup. A MILP formulation, suitably solved by means of SOS2 and SOS1, has been successfully demonstrated. Its simplicity leads to robustness and ease of implementation. The Rainflow counting method was used to determine the most cost effective BESS size with a given operating time, including a 3 kW_P source. This condition (on given operating times) thus needs to be taken into better account for the future operative planning of the basis.

Two 24-h scenarios were analyzed and showed fuel savings in the range of $30-50\%$ with respect to a previous improved configuration. Such approach provides an estimate of the range of fuel savings, should the PV source fail. The analysis of the two scenarios shows that, as long as the operating days of the FOB are below 240 days or above 300, the best size for the BESS is 1 kW (6 kWh capacity), but if the operating days are between 240 and 300, the 3 kW battery (18 kWh capacity) is the best choice.

A laboratory prototype has been built to demonstrate the OEMS functionality. It has also been demonstrated that the OEMS can carry out the commands produced by the optimization algorithm without disturbing the bus voltage to which critical loads are connected. Future work will analyze the impact of adding supercapacitors to the BESS to further increase the battery's lifetime and to service unexpected load transients of short duration.

References

[1] B. Frazee, "Energy symposium looks at reducing the load in marine corps expeditionary operations," Feb. 2010. [Online]. Available: http://www.marforres.marines.mil/MFRNews/NewsArticleDisplay/tabid/7930/Article/81664/

[2] R. Kelly, G. Oriti, and A. Julian, "Reducing fuel consumption at a remote military base: Introducing an energy management system," *IEEE Electrif. Mag.*, vol. 1, no. 2, pp. 30–37, Dec. 2013.

[3] G. Quartarone, M. Liserre, F. Fuchs, N. Anglani, and G. Buticchi, "Impact of the modularity on the efficiency of smart transformer solutions," 2014, pp. 1512–1518. [Online]. Available: https://www.scopus.com/inward/record.uri?eid=2-s2.0-84983097250&doi=10.1109%2fIECON.2014 7048702&partnerID=40&md5=f0f30c6dc2c06379b4f901132e6fb6a2

[4] N. Anglani, G. Oriti, and M. Colombini, "Optimized energy management system to reduce fuel consumption in remote military microgrids," in *Proc. IEEE Energy Convers. Congr. Expo.*, Sep. 2016, pp. 1–8.

[5] C. Hernandez-Aramburo, T. Green, and N. Mugniot, "Fuel consumption minimization of a microgrid," *IEEE Trans. Ind. Appl*, vol. 41, no. 3, pp. 673–681, May 2005.

[6] F. Mohamed and H. Koivo, "System modelling and online optimal management of microgrid using multiobjective optimization," in *Proc. Int. Conf. Clean Elect. Power*, May 2007, pp. 148–153.

[7] C. Chen, S. Duan, T. Cai, B. Liu, and G. Hu, "Optimal allocation and economic analysis of energy storage system in microgrids," *IEEE Trans. Power Electron.*, vol. 26, no. 10, pp. 2762–2773, Oct. 2011.

[8] Q. Fu *et al.*, "Microgrid generation capacity design with renewables and energy storage addressing power quality and surety," *IEEE Trans. Smart Grid*, vol. 3, no. 4, pp. 2019–2027, Dec. 2012.

[9] W. Zhang, F. Lee, and P.-Y. Huang, "Energy management system control and experiment for future home," in *Proc. IEEE Energy Convers. Congr. Expo.*, Sep. 2014, pp. 3317–3324.

[10] F. Berthold, B. Blunier, D. Bouquain, S. Williamson, and A. Miraoui, "Offline and online optimization of plug-in hybrid electric vehicle energy usage (home-to-vehicle and vehicle-to-home)," in *Proc. IEEE Transp. Electrif. Conf. Expo.*, Jun. 2012, pp. 1–6.

[11] F. Fattori, N. Anglani, and G. Muliere, "Combining photovoltaic energy with electric vehicles, smart charging and vehicle-to-grid," *Solar Energy*, vol. 110, pp. 438–451, 2014. [Online]. Available: http://www.sciencedirect.com/science/article/pii/S0038092X14004745

[12] E. Camponogara, K. Campos de Almeida, and R. Hardt, "Piecewise-linear approximations for a non-linear transmission expansion planning problem," *IET Gener. Transm. Distrib.*, vol. 9, no. 12, pp. 1235–1244, 2015.

[13] M. Tankari, M. Camara, B. Dakyo, and G. Lefebvre, "Use of ultracapacitors and batteries for efficient energy management in wind-diesel hybrid system," *IEEE Trans. Sustain. Energy*, vol. 4, no. 2, pp. 414–424, Apr. 2013.

[14] S. Booth and S. Booth, *Net Zero Energy Military Installations: A Guide to Assessment and Planning*. National Renewable Energy Laboratory, Golden, CO, USA, 2010.
[15] G. Oriti, A. Julian, and N. Peck, "Power-electronics-based energy management system with storage," *IEEE Trans. Power Electron.*, vol. 31, no. 1, pp. 452–460, Jan. 2016.
[16] 2016. [Online]. Available: http://www.africapowersystems.com/
[17] 2017. [Online]. Available: https://powersuite.cummins.com/PSWEB/login.action
[18] 2017. [Online]. Available: http://www.sdmo.com/EN/Products/PPR/Power-gen-products
[19] C. Cho, J.-H. Jeon, J.-Y. Kim, S. Kwon, K. Park, and S. Kim, "Active synchronizing control of a microgrid," *IEEE Trans. Power Electron.*, vol. 26, no. 12, pp. 3707–3719, Dec. 2011.
[20] 2016. [Online]. Available: http://lpsolve.sourceforge.net/
[21] E. Beale and J. Forrest, "Global optimization using special ordered sets," *Math. Program.*, vol. 10, pp. 52–69, 1976.
[22] J. Tomlin, "Special ordered sets and an application to gas supply operations planning," *Math. Program.*, vol. 42, pp 69–84, 1988.
[23] M. Miner, "Cumulative damage in fatigue," *J. Appl. Mech.*, 1945. [Online]. Available: http://scholar.google.it/scholar?q=miner+fatigue&btnG=&hl=it&as_sdt =0,5#0
[24] W. Facinelli, "Modeling and simulation of lead-acid batteries for photovoltaic systems," 1983. [Online]. Available: http://scholar.google.it/scholar?q=facinelli+battery&hl=it&as_sdt=0, 5#3
[25] J. Manwell, J. McGowan, W. Stein, and A. Rogers, "Developments in experimental simulation of wind/diesel systems," *Proc. EWEC 1989*, 1989. [Online]. Available: http://scholar.google.it/scholar?q=rogers+wind/diesel&btnG=&hl=it&as _sdt=0,5#3
[26] J. Collins, *Failure of Materials in Mechanical Design, 1981*. Wiley, New York, NY, USA, 1981. [Online]. Available: http://scholar.google.it/scholar?q=Failure+of+Materials+in+Design.+collins+1981&btnG=&hl=it&as_sdt=0,5#0
[27] R. Dufo-López and J. L. Bernal-Agust ín, "Multi-objective design of PV–wind–diesel–hydrogen–battery systems," *Renew. Energy*, vol. 33, no. 12, pp. 2559–2572, Dec. 2008.
[28] R. Dufo-López *et al.*, "Multi-objective optimization minimizing cost and life cycle emissions of stand-alone PV–wind–diesel systems with batteries storage," *Appl. Energy*, vol. 88, no. 11, pp. 4033–4041, Nov. 2011.
[29] 2017. "Genesis 150 np12-12 batteries—specifications," [Online]. Available: http://datasheet.octopart.com/NP12–12-EnerSys-datasheet-10655.pdf
[30] S. Downing and D. Socie, "Simple rainflow counting algorithms," *Int. J. Fatigue*, vol. 4, no. 1, pp. 31–40, Jan. 1982. [Online]. Available: http://www.sciencedirect.com/science/article/pii/0142112382900184
[31] A. Nieslony, "MATLAB central-rainflow counting algorithm," 2010. [Online]. Available: http://scholar.google.it/scholar?hl=it&q=adam+nieslony+Rainflow+Counti ng+Algorithm&btnG=&lr=#2

Norma Anglani (S'93–M'99) received the Laurea (with Hons.) and Ph.D. degrees in electrical engineering from the University of Pavia, Pavia, Italy, in 1993 and 1999, respectively.

After graduating, she worked for a consulting company in the energy efficiency area. She was a Postdoctoral Fellow in the Energy Analysis Group with the Energy Efficiency Standards Group, Lawrence Berkeley National Laboratory, Berkeley, CA, USA. She is currently an Assistant Professor with the Department of Electrical, Computer, and Biomedical Engineering, University of Pavia (I), Pavia, where she currently teaches and does research in the field of energy management, energy planning, modeling, and efficient compressed air systems. There, she set up the Labac Laboratory, University of Pavia, a joint effort between academia and industry. She has been responsible for several research contracts with public and private bodies, and has co-authored more than 60 scientific papers.

Dr. Anglani has been a Chartered Engineer since 1995.

Giovanna Oriti (S'94–M'97–SM'04) received the Laurea (with Hons.) and Ph.D. degrees in electrical engineering from the University of Catania, Catania, Italy, in 1993 and 1997, respectively.

She was a Research Intern at the University of Wisconsin, Madison, WI, USA, for two years. After graduation, she joined the United Technology Research Center, East Hartford, CT, USA, where she developed innovative power converter topologies and control. In 2000, she launched her own consulting business developing physics-based models of power converters and drives for electromagnetic interference analysis, stability analysis, and development of control algorithms. In April 2008, she joined the faculty of the Electrical and Computer Engineering Department, Naval Postgraduate School, Monterey, CA, USA, where she is currently an Associate Professor. Her research interests include power electronics for energy management, microgrids, and renewable energy interface. She holds one U.S. Patent and has co-authored more than 40 papers published in IEEE TRANSACTIONS or IEEE Conference Proceedings.

Dr. Oriti served as the Chair of the Industrial Power Conversion System Department, IEEE Industry Application Society (IAS), in 2011–2012. She received the 2002 IEEE IAS Outstanding Young Member Award. In 2012, she received the Electrical and Computer Engineering (ECE) Department, Naval Postgraduate School (NPS) Service Award in recognition of her contribution to the development of the new NPS Electrical Engineering Energy curriculum. In 2016, she received the NPS ECE Research Award in recognition of her contribution, through her research, to the U.S. Navy's goal of energy efficiency.

Michele Colombini received the Laurea degree in electrical engineering from the University of Pavia, Pavia, Italy, in 2014.

He received a research scholarship for six months to study the technical and economic feasibility of middle-sized steam screw expanders for energy-intensive industrial facilities, such as the paper industry. Since September 2015, he has been with Generac Mobile Products SRL, Villanova d'Ardenghi, Italy, a Generac Power System, Inc. subsidiary, specializing in tower light production. He is currently with the Research and Development Department to develop a new hybrid-fed tower light system, where he is in charge of the simulations for the assessment of the fuel savings due to innovative-fed systems.